HHS Public Access

Author manuscript

Mol Psychiatry. Author manuscript; available in PMC 2022 January 16.

Published in final edited form as:

Mol Psychiatry. 2021 November ; 26(11): 6427–6450. doi:10.1038/s41380-021-01099-w.

Cell-type-specific disruption of PERK-eIF2α signaling in dopaminergic neurons alters motor and cognitive function

Francesco Longo[1], **Maria Mancini**[2], **Pierre L. Ibraheem**[1], **Sameer Aryal**[1,3], **Caterina Mesini**[1], **Jyoti C. Patel**[4,5], **Elena Penhos**[4,5], **Nazia Rahman**[4,5], **Maggie Mamcarz**[1], **Emanuela Santini**[1,6], **Margaret E. Rice**[2,4,5], **Eric Klann**[1,5,°]

[1]Center for Neural Science, New York University, New York, NY

[2]Department Neuroscience and Physiology, NYU School of Medicine, New York, NY

[3]Sackler Institute of Graduate Biomedical Sciences, NYU School of Medicine, New York, NY

[4]Department of Neurosurgery, NYU School of Medicine, New York, NY

[5]NYU Neuroscience Institute, New York University Grossman School of Medicine, New York, NY

[6]Department of Neuroscience, Biomedicum, Karolinska Institute, Stockholm, Sweden

Abstract

Endoplasmic reticulum (ER) stress and the unfolded protein response (UPR) has been shown to activate the eIF2α kinase PERK to directly regulate translation initiation. Tight control of PERK-eIF2α signaling has been shown to be necessary for normal long-lasting synaptic plasticity and cognitive function, including memory. In contrast, chronic activation of PERK-eIF2α signaling has been shown to contribute to pathophysiology, including memory impairments, associated with multiple neurological diseases, making this pathway an attractive therapeutic target. Herein, using multiple genetic approaches we show that selective deletion of the PERK in mouse midbrain dopaminergic (DA) neurons results in multiple cognitive and motor phenotypes. Conditional expression of phospho-mutant eIF2α in DA neurons recapitulated the phenotypes caused by deletion of PERK, consistent with a causal role of decreased eIF2α phosphorylation for these phenotypes. In addition, deletion of PERK in DA neurons resulted in altered *de novo* translation, as well as changes in axonal DA release and uptake in the striatum that mirror the pattern of motor changes observed. Taken together, our findings show that proper regulation of PERK-eIF2α signaling in DA neurons is required for normal cognitive and motor function in a non-pathological

°To whom correspondence should be addressed: Dr. Eric Klann, Center for Neural Science, New York University, 4 Washington Place, Room 621, New York, NY 10003, eklann@cns.nyu.edu.

Author contributions

F.L. carried out the behavioral experiments, performed slice electrophysiology experiments, and collected and analysed all in vivo and ex vivo data. M.M. carried out and analyzed the FSCV experiments. S.A. carried out western blotting and collected ex vivo data. P.L.I. and C.M. carried out behavioral experiments and collected in vivo and ex vivo data. J.C.P. performed DAT-mediated dopamine uptake analysis. M.E.R. coordinated, performed, and analyzed HPLC experiments. E.P. and N.R. carried out HPLC experiments. M.D. performed genotyping of the mice. F.L., E.K., E.S. conceived the studies. M.M. and M.E.R. participated in the design of the studies. F.L. and E.K. designed and coordinated all experiments and wrote the manuscript. All authors read and commented on the paper.

Competing financial interests

The authors declare no competing financial interests.

state, and also provide new insight concerning the onset of neuropsychiatric disorders that accompany UPR failure.

Introduction

Translation control of newly synthesized proteins at the level of initiation is modulated by eukaryotic initiation factor 2α (eIF2α) phosphorylation, which bidirectionally regulates the two major long-lasting forms of synaptic plasticity in the brain: long-term potentiation (LTP) and long-term depression (LTD)[1–3]. Thus, fine-tuning eIF2α phosphorylation levels is instrumental in controlling eIF2α-dependent protein synthesis underlying different learning and memory processes[4–8]. The elF2α alpha kinase protein kinase R-like endoplasmic reticulum kinase (PERK) exerts a critical role in the modulation of protein synthesis-dependent cognitive processes[4–6,9,10]. Selective deletion of PERK in excitatory neurons results in impaired behavioral flexibility[5] and facilitated mGluR-dependent long-term depression (mGluR-LTD)[6]. On the other hand, reducing PERK expression in the cortex or in the CA1 of adult rodent models results in enhanced memory and behavioral flexibility, or in enhanced hippocampus-dependent learning and memory, respectively[9,10]. A recent study points out the central role of PERK in mediating the activity of key metabolic sensors associated with cellular energy homeostasis, disruption of which has been linked to neuronal diseases with cognitive impairments[11].

PERK-dependent phosphorylation of eIF2α upon the accumulation of misfolded and aggregated protein is known to compose one of the three branches of the unfolded protein response (UPR), an integrated signaling pathway that protects cells by restoring normal proteostasis and it is activated by endoplasmic reticulum (ER) stress[12]. UPR signaling controls the overall burden of misfolded proteins through general translational arrest and increased translation of transcription factors that enhance ER protein-folding capacity and quality control through the degradation of proteins with aberrant conformation. Multiple pieces of evidence suggest that the UPR plays a key role in maintaining neuronal function at the level of synapses, connectivity, and brain development[13,14]. Moreover, constitutive activity of the UPR is required in cells with a high secretory load, such as neurons, which leads to increased sensitivity of the brain to abnormalities in the UPR, as well as the duration of its activation[14]. This is reflected in studies of neurodegenerative diseases and psychiatric disorders[15–18], including major depressive disorder (MDD)[19,20], and schizophrenia (SCZ)[21].

PERK phosphorylates eIF2α at serine 51, thereby controlling the initiation step of protein synthesis and subsequently preventing an overload of proteins in the ER lumen[22]. Paradoxically, eIF2α phosphorylation via PERK increases the synthesis of transcription factors that contain upstream open reading frames (uORFs) in the 5’UTR of their mRNAs, including activating transcription factor 4 (ATF4), which is involved in the expression of several UPR target genes[23]. However, when ER stress is sustained and the adaptive mechanisms of the UPR are not sufficient to recover cellular protein homeostasis, a switch to pro-apoptotic signals triggers the death of damaged cells[24], which occurs in neurodegenerative disorders including Parkinson’s disease (PD) and Alzheimer’s disease (AD)[25].

In vitro and *in vivo* studies indicate that UPR activation is a "double-edged sword", as evidence suggests that short-term activation plays a protective role whereas long-term activation results in synaptic failure, impaired synaptic plasticity, and ultimately, cell death[26,27]. Together, these studies reinforce the idea that proper ER proteostasis is key for sustaining neuronal connectivity and function. Activation of the UPR has been reported in post mortem brain tissues from patients with a number of neurodegenerative disorders. Increases in markers of UPR activation, in particular, the increased phosphorylation of PERK and eIF2α, have been observed in PD, AD, and other tauopathies[17,28]. Selective neuronal populations seem to be especially vulnerable to ER stress[29], so it is perhaps unsurprising that the clinical manifestation of neurodegenerative diseases is initiated by the selective alteration in the function of distinct neuronal populations. Activation of PERK-eIF2α signaling and a co-localization of phosphorylated PERK and α-synuclein, a disease-specific misfolded protein, have been reported in dopaminergic (DA) neurons of the substantia nigra in brain tissue of PD patients[28,30]. Beyond its critical role in the control of voluntary movement via the nigrostriatal pathway, DA signaling contributes to synaptic plasticity underlying learning and memory in specific brain regions, including the hippocampus, amygdala, and prefrontal cortex, and altered DA modulation affects the encoding and maintenance of memories[31–33]. Mounting evidence has established that increases in DA function are associated with the onset of psychotic symptoms, a key feature underpinning clinical diagnosis of SCZ[34]. Moreover, either enhanced or reduced DA signaling may be involved in numerous neuropsychiatric disorders such as drug addiction[35], Attention-Deficit/Hyperactivity Disorder (ADHD)[36], Obsessive-Compulsive Disorder (OCD)[37], and Tourette's Syndrome (TS)[38], ASD[39]. Consistent with these findings, targeting the UPR in specific subpopulations of neurons may supply therapeutic benefits in the treatment of diverse neurological disorders.

Given its central role in mediating eIF2-dependent protein synthesis[4,40,41], and in modulating learning and memory processes, is not surprising that PERK-eIF2α signaling has recently emerged as an attractive therapeutic target in several neurological diseases[16,42]. However, these studies have proved to be as controversial as promising[16,43], indicating a new layer of complexity to the involvement of UPR in the diverse pathological manifestations. Nevertheless, very little is known about the effect of PERK reduction specifically in DA neurons and its contribution on motor and cognitive functions remains to be addressed.

In the current study, we explored the cell type-specific modulation of PERK-eIF2α signaling in DA neurons in order to identify the physiological role of PERK in DA neuronal function involved in motor behavior and cognitive processes and to provide insight into how dysregulation of PERK-eIF2 signaling could be involved in neuropsychiatric and neurodegenerative disorders.

We used genetic approaches that included Cre-Lox recombination technology to selectively delete PERK in DA neurons of both the nigrostriatal and mesocorticolimbic pathways to investigate the consequences of manipulating the UPR on motor and cognitive function. Notably, we found that genetic disruption of PERK-eIF2α signaling in DA neurons in mice resulted in multiple motor and cognitive phenotypes. In addition, *de novo* translation studies

revealed dysregulated protein synthesis in DA neurons, and fast-scan cyclic voltammetry (FSCV) in *ex vivo* striatal slices showed an alteration in DA release and uptake that contribute to the behavioral phenotypes caused by the deletion of PERK in DA neurons. Overall, our findings show that proper cell type-specific regulation of PERK-eIF2 signaling in DA neurons is required for normal motor and cognitive function, and that the UPR plays a critical role in maintaining DA neuron function. Furthermore, this study points out the effect of targeting specific component of the UPR on the progression of diverse disorders, depending on the disease context, the neuronal population and the UPR signaling branch that is investigated.

Results

Conditional deletion of PERK in DA neurons leads to multiple motor and cognitive phenotypes in mice.

In order to evaluate whether proper regulation of PERK-eIF2α signaling in DA neurons is required for normal cognitive and motor function, we generated mice containing a DA transporter (DAT) promoter-driven *Cre* transgene (DAT-Cre; Jackson Laboratory, stock number: 006660)[44] and a conditional allele of *Perk* (*Perk*^{loxP}; termed PERK$^{f/f}$; Fig. 1a)[45]. The expression of the *Cre* transgene and the *Perk*^{loxP} allele was determined using PCR-specific primers (Fig. 1b). The resulting conditional knockout mice (PERK$^{f/f}$ DAT-Cre), which lack PERK in DA neurons of both the ventral tegmental area (VTA) and the substantia nigra pars compacta (SNc) represent the primary experimental mouse line used here, along with their littermate control mice (WT DAT-Cre).

Cell-specific deletion of PERK in DA neurons was first verified at the protein expression level by treating coronal midbrain slices containing the VTA and SNc with thapsigargin, which inhibits ER Ca^{2+} sequestration and is a potent inducer of ER stress and eIF2α phosphorylation. Thus, thapsigargin induces the phosphorylation of eIF2α and the expression of ATF4, mainly via activation of PERK. Immunostaining for PERK was clearly seen in tyrosine-hydroxylase positive (TH+) DA neurons in both SNc and VTA in WT DAT-Cre mice, whereas PERK staining was not detected in SNc or VTA DA neurons of PERK$^{f/f}$ DAT-Cre mice, although PERK expression in non-DA (TH-) cells remained intact (Fig. 1c–d). Consistent with these results, downstream UPR targets of PERK such as p-eIF2α (Supplementary Fig. 1a–d) and ATF4 (Supplementary Fig. 1e–f) were significantly reduced in both SNc and VTA DA neurons of PERK$^{f/f}$ DAT-Cre mice compared to thapsigargin-treated controls. Taken together, these results demonstrate a reduced UPR after thapsigargin-induced ER-stress in midbrain DA neurons of PERK$^{f/f}$ DAT-Cre mice, confirming positive targeting of DA neurons for the deletion of PERK.

To provide further verification of the quality of the recombination system and the cell-specificity of *Cre* transgene expression in DAT^{+} neurons, we generated a separate mouse line containing the DAT-Cre transgene, the *Perk*^{loxP} allele and Ai14, a *Cre* reporter allele that has a *loxP*-flanked STOP cassette preventing transcription of a CAG promoter-driven red fluorescent protein variant (tdTomato), all inserted into the *Gt(ROSA)26Sor* locus (B6; 129S6-*Gt(ROSA)26Sor*$^{tm14(CAG-tdTomato)Hze}$; Jackson Laboratory, stock number: 007914)[46] that express tdTomato fluorescence following Cre-mediated recombination (Supplementary

Fig. 2a). Thus, along with the deletion of PERK in neurons in which Cre is expressed (DAT^+ neurons), the STOP cassette is removed and the tdTomato protein is expressed. We found a complete overlap between cells expressing tdTomato fluorescence (Cre-reporter expression) and the DA neuronal marker tyrosine hydroxylase (TH; Supplementary Fig. 2b) in both $PERK^{f/f}$/$CAG^{floxStop\text{-}tdTomato}$DAT-Cre and wild-type (WT)/$CAG^{floxStop\text{-}tdTomato}$DAT-Cre mice. Moreover, we found no staining for PERK in tdTomato co-stained neurons (Supplementary Fig. 2c,e) of $PERK^{f/f}$/$CAG^{floxStop\text{-}tdTomato}$DAT-Cre mice, confirming the specificity of the Cre-recombinase system for the DA neurons. Along with these results, we detected a significant reduction in p-eIF2α levels in DA neurons in both SNc and VTA of $PERK^{f/f}$/$CAG^{floxStop\text{-}tdTomato}$DAT-Cre mice (Supplementary Fig. 2d, f).

To determine consequences of the sustained disruption of PERK-eIF2α signaling in DA neurons on motor ability in mice, we examined $PERK^{f/f}$ DAT-Cre mice and their age-matched WT DAT-Cre littermate controls in a series of behavioral tests. Mice were tested for different motor skills, including akinesia (bar test), bradykinesia (drag test), general motor activity (rotarod test), locomotor activity induced by novelty (NHC), and spontaneous horizontal and vertical locomotor activity in the open field (OF). $PERK^{f/f}$ DAT-Cre mice displayed a hyperactive motor phenotype (Fig. 1e–j). In the bar test, $PERK^{f/f}$ DAT-Cre mice showed reduced immobility time *versus* WT DAT-Cre (Fig. 1e). Consistent with a hyperactive phenotype exhibited in the bar test, $PERK^{f/f}$ DAT-Cre mice showed significantly greater stepping activity than WT DAT-Cre mice in the drag test (Fig. 1f). Motor facilitation was also seen in the rotarod test for PERK mutant mice, with significantly enhanced motor skill acquisition compared to WT DAT-Cre mice (Fig. 1g). Novelty-induced (Fig. 1h) and spontaneous (Fig. 1i) horizontal locomotor activity followed similar patterns, with hyperactivity motor phenotype in $PERK^{f/f}$ DAT-Cre mice compare with their littermate controls (Fig. 1h,i). Moreover, $PERK^{f/f}$ DAT-Cre mice displayed a significantly enhanced vertical locomotor activity in the OF arena compared with their controls (Fig. 1j).

PERK is a key regulator of eIF2-dependent translation, which is a key molecular process underlying learning and memory formation [1,5,10]. To determine whether the conditional deletion of PERK in DA neurons impacts cognitive, as well as motor function, we examined 3- month old $PERK^{f/f}$ DAT-Cre mice and their littermate WT DAT-Cre mice in a series of behavioral tasks to test learning and memory. First, we tested spatial learning and memory in the Morris water maze (MWM), a hippocampus-dependent water escape task. During the acquisition of the hidden platform phase of the water maze task, both genotypes showed a day-to-day decrease in escape latency, although the daily improvement was less in $PERK^{f/f}$ DAT-Cre mice, which consistently exhibited longer escape latencies than WT DAT-Cre controls (Fig. 1k). In a probe test where the platform was removed, $PERK^{f/f}$ DAT-Cre mice spent less time in the target quadrant (Fig. 1l) and crossed the platform location fewer times (Fig. 1m) compared to WT DAT-Cre mice, with representative swim paths shown in Supplementary Fig. 3a. No genotype-specific differences were observed in the average velocity during the MWM test and the visible platform test (Supplementary Fig. 3b,c). The impaired performance observed in mice lacking PERK in midbrain DA neurons suggests that the constitutive disruption of PERK-eIF2α signaling alters a DA-dependent contribution to this hippocampus-dependent spatial memory task.

To confirm our findings that PERK-eIF2α signaling disruption in DA neurons impacts learning and memory, we tested PERK$^{f/f}$ DAT-Cre mice and their WT DAT-Cre littermates on two additional tasks: novel object recognition and an associative threat memory task. In the novel object recognition task, we found that 3-month old PERK mutant mice exhibited similar interactions with familiar objects during training to age-matched WT DAT-Cre mice (Supplementary Fig. 3e), but showed a decreased preference for the novel object, indicating a significantly impaired short-term memory (STM) performance during the test *versus* controls (Fig. 1p). Moreover, young PERK$^{f/f}$ DAT-Cre mice also demonstrated a significantly reduced preference for the novel object *versus* controls when long-term memory (LTM) was examined 24 hours after the test (Fig. 1q). Representative heat maps are shown in Supplementary Fig. 3f. Combined, these results suggest that PERK in DA neurons is important for frontal and temporal cortex-dependent sensory information processing. Similar to the novel object recognition task, 3-month old PERK$^{f/f}$ DAT-Cre mice exhibited altered associative learning and memory when tested with a threat memory task (Fig. 1n,o). Both genotypes performed similarly during training, showing a similar freezing behavior (Supplementary Fig. 3d). However, PERK$^{f/f}$ DAT-Cre mice displayed significantly reduced freezing 24 hours after training for both the context (Fig. 1n) and the cue (Fig. 1o) compared to their WT DAT-Cre littermates. It should be noted that PERK$^{f/f}$ mice show no difference when tested for locomotor activity and cognitive function compared to WT DAT-Cre littermates (Supplementary Fig. 4a–g), further confirming that the multiple motor and cognitive phenotypes exhibited by PERK$^{f/f}$ DAT-Cre mice are attributable to PERK deletion in DA neurons. These behavioral studies indicate that the deletion of PERK in DA neurons not only affects hippocampal and frontal cortex-dependent function but also results in amygdala-dependent memory impairments, suggesting functional alterations of the mesocorticolimbic pathways[47].

Deletion of PERK in DA neurons alters *de novo* translation and multiple behaviors via eIF2α signaling disruption

As mentioned above, phosphorylation of eIF2α on serine 51 is a mechanism through which PERK downregulates global protein synthesis under a variety of cellular stress conditions. Consistent with no expression of PERK, the phosphorylation of eIF2α was reduced in DA neurons of 3-month old PERK$^{f/f}$ DAT-Cre mice (Supplementary Fig. 2d). Given that eIF2α phosphorylation is a key step in translational control under normal physiological conditions and during ER-stress, we investigated the effect of removing PERK on *de novo* protein synthesis in DA neurons (Fig 1r,s; Supplementary Fig. 5). Coronal midbrain slices containing SNc and VTA DA neurons were subjected to fluorescent non-canonical amino acid tagging (FUNCAT) of newly synthesized proteins (Supplementary Fig. 5a). We observed an increase in *de novo* translation in DA neurons of the SNc of PERK$^{f/f}$ DAT-Cre mice compared to wild-type DAT-Cre littermates (Fig. 1r; Supplementary Fig. 5b). Similar to SNc, VTA DA neurons of PERK$^{f/f}$ DAT-Cre mice also exhibited a net increase in newly synthesized proteins (Fig. 1s; Supplementary Fig. 5b).

To confirm that the behavioral results obtained by deleting PERK in DA neurons are due to decreased eIF2α phosphorylation and not due to other cellular functions of PERK, we bred DAT-Cre mutant mice (Jackson Laboratory, stock number: 006660)[44] with conditional

phospho-mutant eIF2α mice[48] (knock-in eIF2α$^{(S51A/\ S51A)}$ mice), where the serine 51 residue has been mutated to alanine (S51A; Fig. 2a). As a result, both the *floxed* wild-type and the mutated eIF2α gene were expressed in all cells of eIF2α$^{(S51A/S51A)}$ DAT-Cre mice, except for the DA neurons (DAT^{+} neurons), where only the mutated eIF2α$^{(S51A/S51A)}$ form is expressed (see Methods section for details). The expression of the *Cre* transgene and the eIF2α$^{(S51A/S51A)}$ allele was determined using PCR-specific primers (Fig. 2b). Then, we verified the cell-specificity of the *Cre* system by treating coronal slices containing the midbrain with thapsigargin to induce ER stress and eIF2α phosphorylation. Levels of p-eIF2α detected by immunofluorescence were significantly reduced (~90%) in both SNc and VTA DA neurons of eIF2α$^{(S51A/S51A)}$ DAT-Cre mice compared to thapsigargin-treated controls (Fig. 2c–d). These data also are consistent with western blotting results showing significantly lower levels of p-eIF2α in both VTA and SNc of eIF2α$^{(S51A/S51A)}$ DAT-Cre mice (Fig. 2e,j). As mentioned above, phosphorylation eIF2α on serine 51 is a mechanism through which PERK downregulates global protein synthesis under a variety of cellular stress conditions. To further confirm the cell-specificity expression of the phospho-mutant eIF2α (eIF2α$^{(S51A/S51A)}$) in DA neurons, we investigated *de novo* translation in DA neurons from thapsigargin-treated midbrain coronal slices with surface sensing of translation (SUnSET). We found a robust increase in *de novo* protein synthesis in both VTA (~50%; Fig. 2f) and SNc (~80%; Fig. 2k) DA neurons of eIF2α$^{(S51A/S51A)}$ DAT-Cre mice compared to controls. Collectively, these data confirm positive targeting of DA (DAT^{+}) neurons for the expression of eIF2α$^{(S51A/S51A)}$ and the disruption of the eIF2α translational control pathway.

We then used the eIF2α$^{(S51A/S51A)}$ DAT-Cre mice and their WT DAT-Cre littermates to investigate whether the motor phenotypes exhibited by PERK$^{f/f}$ DAT-Cre mice are due to the selective reduction of eIF2α phosphorylation in DA neurons. We tested 3-month old eIF2α$^{(S51A/S51A)}$ DAT-Cre mice and their WT DAT-Cre littermates for different motor skills (Fig. 2g–i, l–n). Consistent with the findings with the PERK$^{f/f}$ DAT-Cre mice, we found that conditional phospho-mutant eIF2α mice displayed decreased immobility time in the bar test (Fig. 2g) and greater stepping activity in the drag test (Fig. 2h) than their WT DAT-Cre counterparts. Although we found no effect of the eIF2α conditional phospho-mutation in the rotarod test (Fig. 2i), eIF2α$^{(S51A/S51A)}$ DAT-Cre mice exhibited significantly enhanced horizontal locomotor activity in both the novel home cage (Fig. 2l) and open field arena (Fig. 2m) tasks, as well as greater vertical locomotor activity compared with WT DAT-Cre littermates (Fig. 2n). These findings support the hypothesis that altered general motor ability displayed by the PERK$^{f/f}$ DAT-Cre mice (Fig. 1) is due to the disruption of PERK-eIF2α signaling in DA neurons.

To test the hypothesis that PERK regulates learning and memory via eIF2α phosphorylation control in DA neurons, eIF2α$^{(S51A/S51A)}$ DAT-Cre mice were trained in the same cognitive tasks as the PERK$^{f/f}$ DAT-Cre mice. During MWM training, both genotypes showed a day-to-day decrease in escape latency, but the eIF2α$^{(S51A/S51A)}$ DAT-Cre mice spent significantly longer times to locate the hidden platform (Fig. 3a). eIF2α$^{(S51A/S51A)}$ DAT-Cre mice not only spent less time in the target quadrant (C; Fig. 3b), but also, exhibited a higher preference for the adjacent quadrant (D; Fig. 3b) and crossed the platform location fewer times (Fig. 3c) than their littermate controls in the probe test. No differences in the

visible platform test and the average velocity during MWM test were observed between genotypes (Supplementary Fig. 3h,i). We then tested eIF2α$^{(S51A/S51A)}$ DAT-Cre mice and their littermate controls in the novel object recognition (Fig. 3f,g) and associative threat memory tasks (Fig. 3d,e). During novel object recognition training, 3-month old conditional phospho-mutant eIF2α mice and their controls exhibited similar interaction profile with familiar objects (Supplementary Fig. 3k). No difference in the preference for the novel object was observed between the genotypes during the short-term memory task (Fig. 3f), suggesting intact short-term memory in those mice. However, eIF2α$^{(S51A/S51A)}$ DAT-Cre mice exhibited a reduced preference for the novel object when long-term memory (LTM) was examined 24 hours testing (Fig. 3g). Representative heat maps are shown in Supplementary Fig. 3l. The 3-month old conditional phospho-mutant eIF2α mice also had impaired LTM in the associative threat memory task (Fig. 3d,e). The eIF2α$^{(S51A/S51A)}$ DAT-Cre mice displayed significantly reduced freezing time during contextual (Fig. 3d) and cued (Fig. 3e) testing compared with WT DAT-Cre mice. In addition, eIF2α$^{(S51A/S51A)}$ littermate mice exhibit similar motor and cognitive phenotype compared to WT DAT-Cre mice (Supplementary Fig. 4h–n), confirming that the phenotypes exhibited by eIF2α$^{(S51A/S51A)}$ DAT-Cre mice are due to expression of the phospho-mutant eIF2α specifically in DA neurons. All together, these findings are consistent with the cognitive phenotypes exhibited by the PERK$^{f/f}$ DAT-Cre mice and are consistent with the hypothesis that PERK-eIF2α signaling disruption in DA neurons impacts motor functions and multiple cognitive domains in mice.

Deleting PERK in DA neurons leads to a dysregulation of striatal DA release, DAT activity, synaptic plasticity and DA signaling, without affecting DA content

Midbrain DA neurons project to and modulate multiple highly interconnected modules of the basal ganglia, limbic system, and frontal cortex. Impairment in the DA transmission have been reported not only in PD[49], but also in AD[47] and Huntington's disease (HD)[50], and have been linked to motor as well as cognitive symptoms. Clinical studies have shown that DA abnormalities are also present prior to the onset of psychosis in SCZ[34,51,52], as well as bipolar disorders[53] and ASD[39,54]. Our observation of altered motor and cognitive behavior in PERK$^{f/f}$ DAT-Cre mice led us to hypothesize that the role of PERK in DA neuron function may be critical for proper DA transmission and modulation of the target areas activity. As noted, SNc DA neurons project primarily to dStr and play a critical role in motor function and dysfunction via basal ganglia circuitry[49], whereas VTA DA project to ventral striatum (nucleus accumbens) as well as cortex[32,55] and hippocampus[47]. To provide an index of the effects of selective disruption of the PERK-eIF2α signaling in DA neurons, we used FSCV to quantify single-pulse evoked increases in extracellular DA concentration ($[DA]_o$) and DA uptake in *ex vivo* striatal slices from 3-month old PERK$^{f/f}$ DAT-Cre mice and their littermate controls. Data from the NAc serve as a proxy for expected changes in DA release in other VTA-innervated regions, including the hippocampus. Consistent with motor hyperactivity in 3-month old PERK$^{f/f}$ DAT-Cre mice (Fig. 1e–j), peak evoked $[DA]_o$ in dStr, NAc core, and NAc shell was significantly higher than in littermate controls (Fig. 4a–d). Given that net $[DA]_o$ reflects both DA release and uptake, we determined maximum DA uptake rate, V_{max}, from evoked $[DA]_o$ records. Increased peak evoked $[DA]_o$ could reflect a decrease in V_{max}, for example. However, we found the opposite, with a significantly higher

DA uptake rate in 3-month old PERK$^{f/f}$ DAT-Cre mice in dStr and NAc core (Fig. 4e–h; dStr: 3.23 ± 0.12 μM/s PERK$^{f/f}$ DAT-Cre *versus* 2.29 ± 0.13 μM/s in WT DAT-Cre; NAc: 2.28 ± 0.11 μM/s PERK$^{f/f}$ DAT-Cre vs 1.66 ± 0.10 μM/s control).

Given that altered $[DA]_o$ could reflect changes in DA tissue content, we also determined striatal tissue DA content in the PERK$^{f/f}$ DAT-Cre mice to verify possible changes in DA synthesis that might underlie altered DA availability for release. However, striatal DA levels, quantified using HPLC, did not differ significantly between PERK$^{f/f}$ DAT-Cre mice *versus* their respective controls (Supplementary Fig. 6a–c). Collectively these data show that PERK-eIF2α signaling plays a fundamental role in the dynamic regulation of DA release and uptake, independent of changes in DA synthesis.

Although regulation of axonal DA release in the striatum is often linked to the firing patterns of midbrain DA neurons, the activity of striatal cholinergic interneurons (ChIs) can also trigger axonal DA release independently of DA neuron activity via the activation of nicotinic acetylcholine receptors (nAChRs) on DA axons[56,57]. nAChRs on DA axons are formed by different α and β subunits; previous studies have demonstrated that nAChRs containing β2 subunits mediate ChI-driven DA release[50,58,59]. To verify whether the effects of PERK deletion might involve ChIs and altered nAChR-dependent regulation of DA release, we applied dihydro-β-erythroidine (DHβE; 1 μM) a selective antagonist for β2* subunit-containing nAChRs[50], and again evoked DA release in dStr, NAc core and shell in the same slices recorded under control conditions. The differences in mean peak evoked $[DA]_o$ in PERK$^{f/f}$ DAT-Cre mice *versus* WT DAT-Cre mice persisted in the presence of DHβE, showing that the effect of PERK deletion in DA neurons on axonal DA release is direct and cell-autonomous, and not an indirect effect of altered regulation by ChIs and nAChR activation (Supplementary Fig. 6d–f).

The parallel between changes in locomotor activity in PERK$^{f/f}$ DAT-Cre mice (Fig 1) and changes in evoked DA release (Fig. 4) and uptake in these mice strongly suggests that the modifications in DA release drive the changes in motor behavior. We therefore tested the DA dependence of the behaviors seen in PERK$^{f/f}$ DAT-Cre and WT DAT-Cre mice. Each genotype was challenged with two different doses (0.01 mg/kg, 0.2 mg/kg; i.p.) of the D1 receptor antagonist SCH 23390. We found that acute SCH 23390 (0.01 mg/kg) injection, which previously was shown to cause motor impairments in naive mice[60], was sufficient to induce a reduction in locomotor activity in control mice, but was ineffective in PERK$^{f/f}$ DAT-Cre mice, consistent with enhanced DA release in PERK mutants (Fig. 4i–k). Similarly, PERK$^{f/f}$ DAT-Cre mice treated with low-dose SCH 23390 showed no differences in their stepping activity (Fig. 4i), rotarod performance (Fig. 4j), or distance moved (Fig. 4k), whereas control mice treated with SCH 23390 (0.01 mg/kg) had reduced locomotor activity (Fig. 4i–k). Confirming the DA dependence of motor hyperactivity in PERK$^{f/f}$ DAT-Cre, high-dose SCH 23390 (0.2 mg/kg) reduced locomotor activity in PERK$^{f/f}$ DAT-Cre mice to levels seen in untreated controls (Fig. 4i–k). Taken together, these findings provide strong evidence that the changes in motor activity exhibited by the PERK$^{f/f}$ DAT-Cre mice depend primarily on enhanced DA, and support the notion that similar patterns of DA release alteration may also underlie the changes in cognitive tests observed in PERK$^{f/f}$ DAT-Cre mice.

Previous studies have suggested that DA plays a crucial role in the induction of striatal long-term depression (LTD)[61], one of the two main forms of striatal synaptic plasticity[62,63] at corticostriatal synapses, which depends on the activation of DA receptors[64]. In addition, reduction of evoked DA overflow in the striatum results in a failure to express LTD[65]. Therefore, we determined whether the altered *de novo* translation expressed in PERK-depleted SNc DA neurons underlying the changes in DA release alters striatal LTD in cortico-striatal slices from 3 month-old PERK$^{f/f}$ DAT-Cre and WT DAT-Cre mice. We recorded locally-evoked field excitatory postsynaptic potentials (fEPSPs) in the dorsolateral striatum, then delivered three trains of high-frequency stimulation (HFS) locally to induce LTD. We found that striatal LTD was enhanced in slices from PERK$^{f/f}$ DAT-Cre compared to those from control mice (Supplementary Fig. 5c,d). DA plays a key role in the modulation of hippocampal synaptic plasticity and memory encoding, mostly through its binding to DA receptor[32]. Among the different subcortical inputs, the VTA represents a DA source for the hippocampus[66]. Because our data from the NAc suggested changes in DA release in other VTA-innervated regions, including the hippocampus, and our behavioral results indicated that the disruption of PERK-eIF2α signaling in DA neurons alters hippocampus-dependent learning and memory in the PERK$^{f/f}$ DAT-Cre mice (Fig. 1,3), we examined late-phase long-term potentiation (L-LTP) in hippocampal slices from 3-month old PERK$^{f/f}$ DAT-Cre and control mice. We found that L-LTP, was enhanced in PERK$^{f/f}$ DAT-Cre mice compared to WT DAT-Cre mice (Supplementary Fig. 5e,f). Taken together, these findings suggest that PERK deletion in DA neurons significantly increases *de novo* protein synthesis in both striatonigral and mesocorticolimbic DA neuron populations, alters DA release and results in aberrant expression of both cortico-striatal LTD and hippocampal L-LTP, respectively.

Selective disruption of PERK/eIF2α signaling in SNc DA neurons causes motor phenotypes similar to those exhibited by PERK$^{f/f}$ DAT-Cre mice

DA neurons in the SNc and the VTA play pivotal roles in various brain functions, including the control of motor actions and higher cognitive functions such as learning and memory, motivation, decision-making, and reward processes[49]. These motor functions and cognitive abilities primarily involve two main DA pathways: the nigrostriatal and the mesocorticolimbic pathway, respectively. Thus, we determined whether disrupting PERK-eIF2α signaling in either the DA neurons of the nigrostriatal or the mesocorticolimbic pathway differentially impacted motor function and learning and memory in mice.

We first investigated motor behavior following the selective deletion of PERK in SNc DA neurons. To conditionally delete PERK from DA neurons of the nigrostriatal pathway, we injected either AAV-TH-iCre [67,68] or a control AAV expressing dsRED under TH promoter (AAV-Control) [67] into the SNc of PERK$^{f/f}$ mice (Fig. 5a). To verify the efficacy of PERK deletion, we examined co-expression of PERK and TH in PERK$^{f/f}$ TH-dsRED AAV (control) and PERK$^{f/f}$ TH-Cre AAV mice (Supplementary Fig. 7a–c). In PERK$^{f/f}$ TH-Cre AAV mice, PERK immunofluorescence was observed in ~35% of TH^{+} cells (Supplementary Fig. 7b). Notably, no difference was detected in the total number of TH+ cells between groups (Supplementary Fig. 7c). We subjected PERK$^{f/f}$ TH-Cre AAV mice and their controls to bar, drag, rotarod, NHC, and OF tasks 3 weeks after surgery. We found that mice lacking PERK selectively in DA neurons of the nigrostriatal pathway exhibited a hyperactive motor

phenotype expressed as reduced immobility time in the bar test (Fig. 5c) and higher stepping activity in the drag test (Fig. 5d). In addition, PERK$^{f/f}$ TH-Cre AAV mice performed better than PERK$^{f/f}$ TH-dsRED AAV mice in the rotarod task (Fig. 5e). Moreover, PERK$^{f/f}$ TH-Cre AAV mice exhibited a significant increase in horizontal activity in the NHC task (Fig. 5f) when compared with the control mice. Although spontaneous locomotor activity in the OF task did not differ between PERK$^{f/f}$ TH-Cre AAV mice and controls (data not shown), PERK$^{f/f}$ DAT-Cre mice did show an increase in vertical locomotor activity versus controls (Fig. 5g). We next determined whether deleting PERK in DA neurons of the SNc could affect learning and memory in mice. We found a similar day-to-day decrease in escape latency between genotypes, during the acquisition of the hidden platform version of the Morris water maze (Fig. 5h). Also, no difference between groups was found in the time spent in the target quadrant (Fig. 5i) and in the number of platform crossings (Fig. 5j) in the probe test (Fig. 5i,j), suggesting that hippocampus-dependent spatial memory deficits displayed by the PERK$^{f/f}$ DAT-Cre mice (Fig. 1) are not due to disrupted PERK-eIF2α signaling in SNc DA neurons. No differences between groups were observed in the average velocity during the MWM test and the visible platform test (Supplementary Fig. 8a,b). Moreover, PERK$^{f/f}$ TH-Cre-AAV mice exhibited similar performance compared to the PERK$^{f/f}$ TH-dsRED-AAV control mice when tested in the novel object recognition (Fig. 5k,l; Supplementary Fig. 8d), and the training and LTM contextual threat memory (Supplementary Fig. 8c; Fig. 5m) tasks. Notably, PERK$^{f/f}$ TH-Cre-AAV mice displayed a significant decrease in freezing when compared to the controls during the auditory cue (Fig. 5n), denoting that selective deletion of PERK in SNc DA neurons plays a critical role in cognitive processes and affects amygdala-dependent associative memory in mice. Taken together, these results indicate that PERK$^{f/f}$ DAT-Cre mice exhibit motor phenotypes due to altered function of the nigrostriatal pathway, and impaired associative threat memory that may be related to altered function of the central amygdala (CeA)-SNc-dorsal striatum (dStr) circuitry[69].

Collectively, these data suggest that the loss of PERK in DA neurons of SNc before birth alters control of motor function and importantly, alterations in the nigrostriatal pathway due to the selective deletion of PERK might be detrimental for specific cognitive domains, such as associative threat memory.

Selective disruption of PERK/eIF2α signaling in VTA DA neurons impairs learning and memory

Midbrain DA neurons of the VTA encode multiple signals that influence cognitive processes via diverse projections along mesolimbic and mesocortical pathways. Indeed, VTA projections to prefrontal cortex, hippocampus, amygdala and the ventral striatum are thought to regulate and contribute to various types of learning and memory[32,55]. To conditionally delete PERK from DA neurons of the mesocorticolimbic pathway, we injected AAV-TH-iCre or the control AAV expressing dsRED under TH promoter (AAV-Control) into the VTA of PERK$^{f/f}$ mice (Fig. 5b). We verified the efficacy of PERK deletion by co-expression of PERK and TH in PERK$^{f/f}$ TH-dsRED AAV (control) and PERK$^{f/f}$ TH-Cre AAV mice (Supplementary Fig. 7d–f). We observed PERK immunofluorescence in only ~30% of TH^{+} cells of PERK$^{f/f}$ TH-Cre AAV mice (Supplementary Fig. 7e) and no

difference was detected in the total number of TH^+ cells between groups (Supplementary Fig. 7f).

As expected, selective PERK deletion in DA neurons of the VTA did not alter locomotor activity in mice. Indeed, $PERK^{f/f}$ TH-Cre-AAV mice exhibited similar performance compared to the $PERK^{f/f}$ TH-dsRED-AAV controls when examined in the bar (Fig. 5c), drag (Fig. 5d) and rotarod (Fig. 5e) tests. In addition, no difference was detected between genotypes in either horizontal (Fig. 5f) or vertical (Fig. 5g) locomotor activity. We proceeded to examine learning and memory in $PERK^{f/f}$ TH-Cre AAV and $PERK^{f/f}$ TH-dsRED AAV mice. We found that $PERK^{f/f}$ TH-Cre AAV mice displayed longer escape latencies (Fig. 5h) compared to controls in the training phase of the MWM task. During the probe test, there was no difference between groups in the time spent in the target quadrant (Fig. 5i), but the $PERK^{f/f}$ TH-Cre AAV mice crossed the platform location significantly fewer times than $PERK^{f/f}$ TH-dsRED AAV mice (Fig. 5j). No differences between groups were observed in the average velocity during the MWM test and the visible platform test (Supplementary Fig. 8a,b). Moreover, we found that $PERK^{f/f}$ TH-Cre AAV mice exhibited a reduced preference for the novel object in both STM (Fig. 5k) and LTM (Fig. 5l) tests in the novel object recognition task. Both groups showed similar interaction time during training (Supplementary Fig. 8d). The selective deletion of PERK in the VTA DA neurons also recapitulated impaired associative memory deficits exhibited by the 3-month old $PERK^{f/f}$ DAT-Cre mice in the associative threat memory tasks. $PERK^{f/f}$ TH-Cre AAV mice displayed similar freezing behavior during training (Supplementary Fig. 8c) but significantly decreased freezing time when exposed to the context (Fig. 5m) and the auditory cue (Fig. 5n) compared to their controls, consistent with the idea the disruption of PERK-eIF2α signaling in VTA DA neurons impacts several cognitive domains in a similar manner to mice.

Discussion

The upregulation of PERK-dependent UPR markers has emerged as a consistent feature of multiple neuropsychiatric disorders, with particular focus on neurodegenerative diseases over the last decade[15,17,19–21]. Evidence of dysregulated PERK-eIF2α signaling in *post-mortem* brain tissues of PD and AD patients[28], as well as in preclinical models[70,71] of neurodegenerative disease, marked a turning point in the recent research strategy on neurodegenerative disorders, bringing into focus the therapeutic value of UPR modulation across the spectrum of these diseases. Chronic activation of PERK signaling via eIF2α phosphorylation is thought to alter neuronal function by repressing global protein synthesis, particularly the synthesis and expression of a cluster of proteins important for the establishment of synapses and neuronal plasticity[41]. This type of PERK-eIF2α-dependent translation might account not only for synaptic failure, but also for and subsequent cognitive decline observed in most neurodegenerative disorders[1,72,73]. Thus, it is perhaps unsurprising that modulation of the PERK-eIF2α signaling has emerged as a promising therapeutic target for neurodegenerative disease. Much of the research focus regarding either pharmacological or genetic inhibition of PERK signaling to reduce p-eIF2α levels has been placed on models of pathology, suggesting a neuroprotective effect of restored eIF2α-dependent translation in mice [41,74–76]. However, there is other evidence from studies of preclinical models of neurodegenerative disorders that depict a complex scenario where, depending

on the disease context, modulation of PERK-branch mediated translational control may result in contrasting and even opposite effects[16,43,77]. In line with this, lower levels of PERK expression have been reported in the dorsolateral prefrontal cortex in patients with SCZ[21], whereas preclinical models of multiple neuropsychiatric disorders exhibit higher levels of phospho-eIF2α, a finding attributed to increased PERK activation[78]. Moreover, a recent study reported that PERK expression and its activity is severely decreased in DA neurons of individuals with 22q11.2 deletion, one of the most common microdeletion syndromes in humans and an extremely high-risk genetic factor for various neuropsychiatric disorders including intellectual disability and SCZ [79]. Thus, to fully understand the role of the UPR in pathology and normal brain function, dissecting the impact of modulating the PERK-eIF2α translational control pathway in a cell type-specific manner is necessary, especially if this pathway is to be harnessed as a therapeutic target to treat neuropsychiatric and neurodegenerative diseases. In this study, we provide evidence that cell type-specific deletion of PERK in midbrain DA neurons results in multiple motor and cognitive phenotypes in mice. Our current study is the first demonstrating, that sustained reduction of PERK-eIF2α signaling in DA neurons affects DA release and subsequently, DA signaling that impacts both nigrostriatal and mesocorticolimbic pathways.

Classically, eIF2α-mediated translational control in the brain has been studied in the context of synaptic plasticity as well as learning and memory processes[23,80], with most of the studies focusing on molecular manipulation in excitatory neurons[4,5,10]. Our findings reveal a previously unrecognized role of PERK-eIF2α-mediated translation in DA neurons and provide molecular insights into the pathophysiology of motor and cognitive impairments when this type of translational control is disrupted. We found that reduced eIF2α phosphorylation in midbrain DA neurons leads to increased *de novo* translation, which results in DA dysfunction as well as multiple motor and cognitive impairments. Notably, there is an extensive body of literature describing the differential gene and protein expression between different DA neuron populations, which could underlie their selective vulnerability in the context of different neurological disorders[47,81]. *De novo* protein synthesis was markedly increased in TH^+ neurons of both the SNc and the VTA at 3 months of age, consistent with a clear dysfunction in both nigrostriatal and mesocorticolimbic pathways. Both pre- and postsynaptic protein synthesis is required for striatal LTD[62,63], which depends on the activation of DA receptors[63,64], as does locomotor behaviors, action selection, and associative learning[82]. The hyperactive motor phenotype exhibited by $PERK^{f/f}$ DAT-Cre mice is correlated with enhanced cortico-striatal LTD (Supplementary Fig. 5c,d), likely via D2 receptor activation[83], and elevated DA release in the dorsolateral striatum, as indicated by FSCV data (Fig. 4). Notably, preclinical models of PD, where degeneration of SNc DA neurons leads to striatal DA depletion, show impairment in indirect pathway mGluR-LTD[84]. The inhibition of indirect pathway LTD causes a shift of balance toward direct pathway LTP in the striatum, which ultimately inhibits movement[63]. Although DA binds to both D1 and D2 receptors, the activation of either subtype depends on the amount of DA release and the respective affinities of the receptors for DA[49]. Either hyperdopaminergic or hypodopaminergic states can drive the system to become imbalanced, leading to unidirectional changes in plasticity that could underlie network pathology and symptoms[84].

Despite no changes in DA content, PERK-deficient DA neurons showed increased DA release and uptake in the dStr and NAc of young PERK$^{f/f}$ DAT-Cre mice that correlated with a marked hyperactive motor phenotype and required a higher dose of SCH-23390 to block D1 receptors, than that sufficient to induce changes in behavior in WT DAT-Cre mice (Fig. 4). Consistent with this notion, preclinical models of SCZ are characterized by a prominent hyperlocomotion, which is a rodent correlate of positive symptoms of SCZ, and that was largely resistant against D1-receptor antagonism[85]. Our findings suggest that PERK is important for the regulation of DA release and reuptake activity. Indeed, selectively deleting PERK from SNc DA neurons postnatally using a viral approach led to enhanced locomotor activity (Fig. 5), which is consistent with the motor phenotype exhibited by PERK$^{f/f}$ DAT-Cre mice (Fig. 1). Curiously, selective deletion of PERK in SNc DA neurons resulted in an amygdala-dependent memory impairment (Fig. 5), which is consistent with the dense interconnections between the SNc and CeA identified as part of a CeA-SNc-CPu loop that underlies associative learning[69].

It is well established that DA regulation of basal ganglia circuitry occurs mainly in the striatum, the major input nucleus that also plays a central role in processing motivational, associative and sensorimotor information[86]. Increased subcortical dopamine synthesis and release capacity are strongly associated with positive symptoms in SCZ patients where PET imaging found that increases synaptic dopamine content, and synthesis capacity were localized, or more pronounced, in the associative striatum[34]. The increase in eIF2α-dependent translation via PERK deletion in VTA DA neurons is also correlated with an increase DA release and uptake in the NAc (Fig. 4). DA plays a key role in the modulation of multiple forms of learning and memory by acting upon specific brain regions, including the hippocampus, amygdala, and prefrontal cortex, and altered DA signaling has been shown to impair the encoding and maintenance of memories[31–33]. Altered DA signaling resulting from PERK deletion in VTA DA neurons may compromise the role of DA in the modulation of those target structures, ultimately resulting in impaired learning and memory. Indeed, DA is required for late-phase long-term potentiation (LTP) and spike timing-dependent plasticity in the hippocampus[87], and DA receptor signaling regulates aversive memory retention[32]. Consistent with these observations, we found that hippocampal L-LTP is enhanced in PERK$^{f/f}$ DAT-Cre mice (Supplementary Fig. 5e,f) and hippocampus-dependent contextual memory is altered in PERK$^{f/f}$ DAT-Cre mice (Fig. 1), indicating that PERK activity in DA neurons is critical for encoding contextual information. Pharmacological activation of D1/D5 receptors, gates long-term changes in synaptic strength and facilitates induction and duration of LTP at CA1 and dentate gyrus synapses of the dorsal hippocampus in vivo[88]. In addition, DAT re-uptake blockade, which increases DA availability, results in increased LTP magnitude in area CA1 of the rat hippocampus[89]. PERK deletion, specifically in DA VTA neurons, results in spatial learning and memory impairments in the MWM task (Fig. 5). In agreement with these findings, it has been shown that proper mesocorticolimbic DA neuronal function promotes hippocampal network dynamics associated with memory persistence[90] and DA in the hippocampus has been shown to play a role in plasticity underlying spatial novelty[91]. The main DA input to the hippocampus arises from the VTA, which has been postulated to form a loop with the hippocampus that then regulates the activity of the VTA to control hippocampal activity through the release of DA[92]. Moreover,

deletion of PERK in excitatory neurons in the forebrain was shown previously to cause impaired cognitive function, especially in behavioral flexibility[5]. Finally, a reduction of eIF2α phosphorylation in mice lacking the eIF2α kinase GCN2[72] results in a robust L-LTP after HFS in the hippocampus and impairments in long-term memory in standard learning and memory paradigms. However, in $eIF2\alpha^{+/S51A}$ mice, the threshold for eliciting L-LTP in hippocampal slices is lowered, and memory is enhanced[1].

We also found that $PERK^{f/f}$ DAT-Cre mice exhibit a preference for the familiar rather than the novel object in the novel object recognition test (Fig. 1), suggesting that impaired PERK-eIF2α signaling in VTA DA neurons results in prefrontal cortex information processing deficits. DA modulation in the prefrontal cortex is crucial for object recognition memory and the dysfunction of the dopaminergic system contributes to age-related cognitive decline in AD model mice[93]. Moreover, the consolidation of object recognition memory requires simultaneous activation of dopamine D1/D5 receptors in the amygdala and medial prefrontal cortex[94]. Consistent with this notion, we showed that deleting PERK selectively in VTA DA neurons with a viral approach results in impaired spatial, associative, and discriminative memory in mice (Fig. 5). Our results suggest that PERK-eIF2α signaling is essential for proper function of mesecorticolimbic DA neurons early in life, and, therefore, it may also play a key role in the regulation of VTA DA neuron function in the adult DA system. Moreover, we can speculate that a sustained reduction of eIF2α phosphorylation, may be detrimental for the integrity of DA signaling and either an increase or a reduction of DA outflow levels negatively affects DA neurons modulation of target structures. Notably, clinical studies have shown patients with SCZ exhibit increased presynaptic dopamine function in the associative striatum, which are present prior to the onset of psychosis[34]. Different cognitive symptoms including impaired attention and cognitive control may involve excessive levels of DA in the striatum, but reduced DA amounts in PFC in SCZ individuals[95]. Nevertheless, over activation of the dopaminergic system in SCZ patients underlying the presence of psychosis, correlates with an hyperactivation of the hippocampus which is associated with a dysregulation of the loop formed by the thalamus, hippocampus, and VTA in those individuals[96]. Moreover, a recent study on cognitive deficits displayed by AD model mice pointed out the link between alteration in VTA DA neurons and deficits of hippocampus-dependent memory and synaptic plasticity[47]. It has been shown that a decrease in DA in the hippocampus and NAc shell of AD model mice due to VTA DA neuronal degeneration results in impaired synaptic plasticity, memory performance, and food reward processing, which suggests that altered VTA DA neuron function contributes to cognitive deficits in AD[47].

UPR activation has been described as a “double-edged sword” because short-term activation plays a protective role whereas sustained activation results in synaptic failure, impaired synaptic plasticity, and ultimately, cellular death[26,27]. Interestingly, multiple studies on neurodegenerative disease support the notion that prolonging, rather than inhibiting, PERK-eIF2α signaling results in neuroprotective effects. For example, in the A53T alpha-synuclein mutation model of PD, activation of the PERK branch mediates a pro-survival response[97] and blocking eIF2α dephosphorylation in mutant SOD1 G93A mice, an amyotrophic lateral sclerosis (ALS) mouse model, prevents motor neuron degeneration and aggregation of mutant SOD1[98]. Thus, enhancing the PERK pathway by selectively

inhibiting GADD34-mediated dephosphorylation of eIF2α in mutant model of SOD1 mice appears to significantly ameliorate the disease condition[99]. A recent study on multiple forms of dystonia, a brain disorder associated with involuntary movement and DA deficiency, demonstrated reduced eIF2α signaling in DYT1 dystonia patient-derived cells and that enhancing eIF2α signaling restored abnormal corticostriatal synaptic plasticity in a DYT1 mutant mouse model[77]. Notably, a recent clinical study indicates that dysregulation of the UPR and consequent alterations in protein processing contribute to the pathogenesis of SCZ. It has been shown that among other key sensors of the UPR, PERK expression was decreased in the dorsolateral prefrontal cortex of elderly patients with SCZ, suggesting also that PERK pathway is sensitive to aging and likely underlies an altered capacity to deal with ER stress in elderly individuals[21]. Nevertheless, data from both mouse models and patient-derived iPSCs show that reduced PERK expression and activity represent a key factor that contributes to the 22q11.2DS-related brain pathology in DA neurons, resulting in SCZ-like cognitive dysfunction in mice, and poor tolerance to ER stress and abnormal F-actin dynamics[79].

In closing, our findings reveal the importance of PERK-eIF2α-mediated translational control in DA neurons and its role in normal motor function and in learning and memory. Moreover, given the general agreement that preventing translational repression caused by increased eIF2α phosphorylation might be beneficial for treatment of cognitive deficits associated with neurodegenerative disorders, our study sheds light on the consequences of disruption of PERK in DA neurons for motor and cognitive function in a non-pathological condition. Moreover, pave the way for cell type-specific dissection of the role of PERK, as well as the UPR, in the study of different neurological diseases. Finally, our study is not merely limited to the evaluation of the effect of PERK-eIF2α-mediated translational control repression but uncovers an entirely new biological link between PERK and DA neuronal function that is involved in motor behavior and cognitive. Further investigation is needed to elucidate how disruption of PERK-eIF2α signaling affects general and gene-specific translation in DA neurons to alter DA release and uptake and ultimately, motor and cognitive behavior. The clarification of cell type-specific physiological UPR control may provide new insight on the onset of diseases that accompany UPR failure and to the development of novel therapeutic methods that target the UPR among several neuropsychiatric disorders.

Methods

Animals.

All mice were housed in groups of 3–4 animals per cage in the Transgenic Mouse Facility of New York University and maintained in accordance with the US National Institutes of Health Guide for Care and Use of Laboratory Animals. The facility was kept under regular lighting conditions (12 h light/dark cycle) with a regular feeding and cage-cleaning schedule. Mice were all maintained on a C57/BL6 genetic background and all genotypes were determined by polymerase chain reaction (PCR). Randomization was not used in animal studies.

Transgenic mice obtained by selective ablation of PERK in midbrain DA neurons were generated by crossing mice harboring floxed PERK gene, *Eif2ak3* ($PERK^{f/f}$; generated

as previously described; Zhang et al. 2002) with heterozygous DAT-Cre recombinase mouse line (Jackson Laboratory, stock number: 006660)[44] expressing *Cre* recombinase inserted upstream of the first coding ATG of the dopamine transporter gene (*Slc6a3*; DAT). As reported by the Jackson Laboratory, the Cre recombinase activity is observed as early as embryonic day 15, and co-localizes with endogenous gene expression in adult dopaminergic cell groups (substantia nigra (SN) and ventral tegmental area (VTA). The resulting heterozygous mice ($PERK^{f/+}$ DAT-Cre) were crossed with $PERK^{f/+}$ mice in order to obtain PERK DA conditional knockout ($PERK^{f/f}$ DAT-Cre) mice and, the respective wild-type (WT DAT-Cre) littermates mice used as a control.

Knock-in $eIF2\alpha^{(S51A/\ S51A)}$ mice expressing transgenic floxed wild-type *eIF2s1* gene were kindly provided by Dr. Randal J. Kaufman and generated as previously described[100]. The generation of $eIF2\alpha^{(S51A/S51A)}$ DAT-Cre mice, where the serine 51 residue has been mutated to alanine (S51A) selectively in DA neurons required two stages of breeding. First, $eIF2\alpha^{(S51A/+)}$ DAT-Cre mice were obtained by crossing $eIF2\alpha^{(S51A/\ S51A)}$ mice with heterozygous DAT-Cre recombinase mouse line (Jackson Laboratory, stock number: 006660). Second, $eIF2\alpha^{(S51A/+)}$ DAT-Cre mice were crossed with $eIF2\alpha^{(S51A/+)}$ to generate conditional phospho-mutant eIF2α mice $eIF2\alpha^{(S51A/S51A)}$ DAT-Cre mice and, the respective wild-type (WT DAT-Cre) littermates mice used as a control. The resulting $eIF2\alpha^{(S51A/S51A)}$ DAT-Cre mice express both the floxed wild-type and the mutated eIF2α gene in all cells except for DA neurons (DAT+ neurons), where only the mutated eIF2α(S51A/S51A) form is expressed since the wild-type eIF2α gene is excised by *Cre*.

$CAG^{floxStop\text{-}tdTomato}$(Ai14) conditional reporter line (B6; 129S6-*Gt(ROSA)26Sor*$^{tm14(CAG\text{-}tdTomato)Hze}$; Jackson Laboratory, stock number: 007914)[46] and $PERK^{f/+}$ DAT-Cre mice were crossed to generate $PERK^{f/f}$/$CAG^{floxStop\text{-}tdTomato}$DAT-Cre mice and $PERK^{+/+}$/$CAG^{floxStop\text{-}tdTomato}$ DAT-Cre (named $CAG^{floxStop\text{-}tdTomato}$ DAT-Cre) mice expressing tdTomato fluorescence following Cre-mediated recombination in DAT^{+} neurons. Mice generated from this cross were used exclusively to confirm the specificity of the Cre-recombinase system for the DAT^{+} neurons and the consequential deletion of PERK in dopaminergic neurons by immunofluorescence.

AAVs infusion.

AAV2/10-TH-iCre and AAV2/10-TH-dsRED adeno-associated viruses (~10^{12} infectious units ml^{-1}) were kindly provided by Dr. Caroline Bass and were generated as previously described[67]. Briefly, mice were anesthetized with a solution of ketamine hydrochloride (100 mg/kg, i.p.) and xylazine (10 mg/kg, i.p.), mounted onto a stereotaxic apparatus and viruses were infused bilaterally at the rate of 0.1 µl/min. Microinjection needles were left in place for an additional 5 min to allow for diffusion of viral particles. $PERK^{f/f}$ mice were injected at either 2 or 11 months of age and allowed three weeks to recover after surgery. Injection coordinates targeting the SNc or the VTA were as follows (with reference to bregma): −3.1 AP, ± 1.2 ML, −4.3 DV (SNc) or −3.50 AP, ± 0.35 ML, −4.50 DV (VTA).

Experimental design.

For all behavioral and molecular experiments, mice of either sex were used. Mice subjected to locomotor activity and cognitive skills analysis were tested at 3 months. $PERK^{f/f}$ mice (2 months of age) were subjected to intracranial injections of AAV-TH-Cre or AAV-dsRED in either the SNc or the VTA and tested for both motor and cognitive skills 3 weeks after AAV infusions. All mice were acclimated to the testing room 30 min prior to each behavioral experiment and all behavioral apparatuses were cleaned with 30% ethanol between each trial. The experimenter was blind to genotype. All behavioral tests were performed starting with the least aversive (locomotor activity) and ending with the most aversive (associative threat memory task) task.

Mouse behavior: bar test.

Originally developed to quantify morphine-induced catalepsy, this test measures the ability of the animal to respond to an externally imposed static posture. It can also be used to quantify akinesia (i.e. time to initiate a movement) also under conditions that are not characterized by increased muscle tone (i.e. rigidity) as in the cataleptic/catatonic state. Mice were gently placed on a table and forepaws were placed alternatively on blocks of increasing heights (1.5, 3 and 6 cm). The time (in seconds) that each paw spent on the block (i.e. the immobility time) was recorded (cut-off time of 20 s). Performance was expressed as total time spent on the different blocks. The test was performed in two consecutive days[101].

Mouse behavior: drag test.

This test gives information regarding the time to initiate (akinesia) and execute (bradykinesia) a movement. It is a modification of the ‘wheelbarrow test’, and measures the ability of the animal to balance its body posture with the forelimbs in response to an externally imposed dynamic stimulus (backward dragging). Animals were gently lifted from the tail leaving the forepaws on the table, and then dragged backwards at a constant speed (about 20 cm/s) for a fixed distance (100 cm). The number of steps made by each paw was recorded. Five determinations were collected for each animal. The test was performed on two consecutive days[101].

Mouse behavior: rotarod test.

The accelerating rotarod task (UGO BASILE, Biological Research Apparatus) was used to test balance and motor coordination. The rotarod test was performed by placing mice on a rotating drum (3 cm of diameter), and measuring the time that each mouse was able to achieve walking on the top of the rod. The time at which each animal fell from the drum, touching the plate at the base of the rod, was recorded automatically. If the mouse stopped walking, the session was considered ended at the third full turn of the drum without movement. The speed of the rotarod accelerated from 4 to 40 RPM over a 5 min (300 sec) period. Mice were given 4 consecutive trials with a maximum time of 300 sec and a minimum of 15 min inter-trial for two consecutive days. The fall latency (expressed in sec) obtained from each of 4 trials of the two days was used for statistical analysis[102].

Mouse behavior: novel home cage test (NHC).

The NHC test was used to assess the spontaneous horizontal motor activity as novelty-induced exploratory response. Mice were placed in a 35 × 22 × 22 cm experimental cage with the floor covered with bedding. Locomotor activity (expressed in cm) was recorded over a 60 min period by using a computerized video tracking system (Noldus, EthoVision XT 13)[103]. The parameter tested was the total distance traveled during the test and in each of the 6 intervals of 10 min.

Mouse behavior: open field (OF) test.

The OF test was used to measure the spontaneous general locomotor activity and anxiety-like behavior[104]. Mice were placed in the center of a clear Plexiglas open field (40 × 40 × 30 cm) for 15 min and a computer-operated optical system (Activity Monitor software for Open Field) monitored the movement of the mice as they explored in the open field. The parameters tested were: total distance traveled, vertical counts (expressed as % of control). The data were pooled according to genotype, and a mean value was determined for each group.

Mouse behavior: novel object recognition task.

The novel object recognition task was performed to analyze both STM and LTM[102]. Two familiar objects with same shape (2.5 × 2.5 × 2.5 cm) and color were used during habituation days. Objects with different shape (2.5 × 2.5 × 5 cm) and color from the familiar object, were used as novel objects. STM novel object was rectangular shaped and LTM novel object was round shaped. Mice were habituated to the arena and to the two familiar objects (FO) for 2 consecutive days and for 10 min each day. The following day, mice were exposed to the arena with the same two identical objects for the third time and the interaction time with both the objects was recorded (Noldus, EthoVision XT 13) during a 10 min period. After 1 hour, mice were tested for STM and they were exposed to the arena with one FO and the novel object (NO) replaced the non-preferred familiar object. Interaction time with both the objects was recorded for 5 min period. On day 4, mice were tested for LTM and the STM novel object was replaced with the LTM novel object; interaction time with both the objects was recorded for 5 min period and analyzed with the computer program. Interaction parameters were defined as contact with the object (noise-point detector; distance ≤ 2.54 cm). The Preference Index (PI) was calculated using the following equation:

$$PI = (\textit{time interacting with NO})/(\textit{time interacting with NO} + \textit{time interacting with FO})$$

Mouse behavior: Morris water maze.

The Morris water maze test (MWM) was used to study spatial memory associated to a context. The maze consisted of a circular pool (52 cm in diameter) filled with water, and colored with white non-toxic paint to increase the water's opacity. The pool was separated into four virtual quadrants. There were both proximal as well as distant visual cues in place. There were visual cues placed both on the pool and around the room to mark the position of the different quadrants and a hidden platform was placed in one quadrant. The diameter

of the platform was 10.5 cm, which was 1 cm beneath the surface of the water. On days 1–5, mice were trained to locate the hidden platform. The training phase consisted of four (day 1) or 3 (day 2–4) trials per day with a cutoff of 60 sec and 15 min of inter-trials interval. On each day, the swim start positions for each trial were placed sequentially and counterclockwise in the quadrants, allowing mice to start from all the positions at the end of the training phase. The latency to find the platform was recorded. On day 5 mice were subjected to a 60 sec probe trial where the platform was removed from the pool. The parameters measured during the probe trial (also referred as test), were the number of platform crossings and time spent in each quadrant. One hour and a half after the probe trial, visible platform test was performed to ensure that none of the mice were impaired in their visual acuity. The platform was replaced in the same position as the training phase and a small flag was placed on the top of it to indicate the platform position, and the latency to find the visible platform was measured[102]. Escape latency, number of previous platform position crossings, time spent in each quadrant, and trajectories of the mice in the Morris water maze task were recorded with a computerized video tracking system (Noldus, EthoVision XT 13).

Mouse behavior: associative threat memory task.

Contextual and cued threat conditioning (TC) was used to measure associative fear memory[105]. Mice were subjected to a neutral stimulus or context called “conditional stimulus” (CS), a 30 sec 80 dB tone; and an aversive stimulus called “unconditional stimulus” (US), a 2 sec 0.5 mA foot shock. Mice received two day of habituation (900 sec) to the training context, consisting of a white house light and metal conducting grid floor. On the training day mice were placed in the TC chamber (570 sec) and then given two sequences of CS-US, the first at 270 sec and the second at 420 sec. In this session mice associated the aversive experience (US) to the noise (CS). Freezing time was measured for intervals: from the start to the first CS-US (270 sec), during the first CS-US (30 sec), from the end of first CS-US to the second one (120 sec), during the second CS-US (30 sec) and from the end of second CS-US to the end (120 sec). On day 3, mice were probed first for context TC and then for cued TC, with one hour and a half interval. In context TC, mice were exposed to the training context as the habituation day (without foot shock and tone), and recorded for 300 sec; freezing time was measured every interval of 60 sec. In this session mice remembered the environment where they received the aversive stimulus. Cued TC was measured by placing mice in a novel context consisting of a red house light, a white Plexiglass floor and vanilla flavored bedding; cleaning solvents also was changed with 30% isopropanol. Mice were recorded for 720 sec and they were given three CS at 270 sec, 440 sec and 570 sec. Freezing time was measured in intervals: from 0 sec to 270 sec, during the first CS (30 sec), from the end of the first CS to the second CS (140 sec), during the second CS (30 sec), from the end of the second CS to the third CS (100 sec), during the third CS (30 sec), and finally from the end of the third CS to 720 sec (120 sec). Habituation, context TC and cued TC protocols, videos recording and freezing time analysis were performed with FreezeFrame™ software (version 4.08, Actimetric Inc).

Behavioral pharmacology.

Three-month-old PERK$^{f/f}$ DAT-Cre and WT DAT-Cre mice were acutely administered i.p. with the DAT inhibitor GBR-12783 dihydrochloride (Tocris Bioscience, cat no: 0421) at a doses of 6 or 10 mg/kg, the VMAT2 inhibitor reserpine (Tocris Bioscience, cat no: 2742) at a dose of 1 or 1.5 mg/kg, or the D1 receptor antagonist SCH 23390 hydrochloride (Tocris Bioscience, cat no: 0925) at a dose of 0.01 or 0.2 mg/kg, and motor activity was assessed using the drag, the rotarod, and the open field tests. Mice were tested 20 min (GBR-12783; SCH 23390) or 24 hr (reserpine) after drug administration. Experimenters were blind to the genotype and treatment.

Fluorescent labeling of *de novo* protein synthesis in DA neurons.

A fluorescent non-canonical amino acid tagging (FUNCAT) method was used to detect changes in *de novo* protein synthesis in DA neurons and it was performed as previously described[106] with minor modifications. Briefly, 400 μm transverse slices were incubated with azido-homoalanine (AHA) at 32°C for 2.5 hours. At the end of the incubation slices were transferred into ice-cold 4% PFA for overnight fixation at 4°C. The following day, slices were mounted in 3% agarose and sliced using a vibratome (Leica VT1200S; Leica Microsystems; Bannockburn, IL) to a thickness of 30 μm. Free floating sections were collected in Tris-buffered saline (TBS), washed, blocked and permeabilized with 5% bovine serum albumin (BSA), 5% normal goat serum (NGS), 0.3% Triton-X-100 in TBS for 90 minutes (at RT). Slices were then washed with TBS and incubated with 500 μl of cyclo-addition reaction mix (Click-iT™ Cell Reaction Buffer Kit, Invitrogen, Ltd, Paisley, UK) for overnight cyclo-addition at 4°C with gentle rocking. Then, slices were rinsed in TBS, blocked in 1% NGS solution in TBS, and incubated with anti-tyrosine hydroxylase (TH) antibody (Millipore, MA, United States, cat no: MAB318). Slices were then rinsed in TBS and incubated with Alexa Fluor™488 goat anti-mouse secondary antibody (Invitrogen, Carlasbad, CA, USA). Finally, slices were rinsed with TBS and mounted using DAPI fluoromount-G™ (Electron Microscopy Sciences, Hatfield, PA, USA). AHA was detected using an Alexa Fluor™ 647 Alkyne, Triethylammonium Salt (Invitrogen, Carlasbad, CA, USA) and subsequent fluorescence imaging.

Immunofluorescence and confocal microscopy.

Mice were perfused intracardially with phosphate-buffered saline (PBS) followed by 4% paraformaldehyde. Brains were removed and stored in the same fixative o.n. at 4°C. The immunofluorescent staining was performed on 40-μm thick free-floating coronal midbrain slice containing VTA and SNc DA neurons that were prepared using a vibratome (Leica VT1200S; Leica Microsystems; Bannockburn, IL). For identification of DAT-specific deletion of PERK and consequential reduction of phosphorylated eIF2α (p- eIF2α) levels in VTA and SNc DA neurons, sections were blocked in 0.1% Triton-X-100, 5% NGS in TBS for 1h and incubated with primary antibodies o.n. at 4°C. The following primary antibodies were used: anti-tyrosine hydroxylase (TH) antibody (Millipore, MA, United States, cat no: MAB318) phospho-eIF2α (Ser51; Cell Signaling Technology, cat no: 33985), PERK (Cell Signaling Technology, cat no: 3192), anti-dsRED antibody (Thermofisher, cat no: 632496), anti-ATF4 (Santa Cruz, cat no: sc-390063). Alexa Fluor™ 488 or 647

secondary antibodies (Invitrogen, Carlasbad, CA, USA) were used. Sections were mounted using ProLong TM Gold Antifade mounting medium without DAPI (Invitrogen, Thermo Scientific, cat no: P36930). The sections were imaged using a Leica TCS SP8 confocal microscope (Leica, Germany) at 10X or 20X objective lens. All parameters (pinhole, contrast, gain and offset) were held constant for all sections from the same experiment. For analysis of AHA-Alexa-647 signal, 40 regions of interest (ROI) corresponding to soma size were selected from 20x TH-Alexa-488 images and were then measured in AHA-Alexa-647 images. Arbitrary fluorescent units (a.u.) were taken from Z-stack acquired images from the minimum value in the ROI to preserve the dynamic range as the increase in fluorescence between $PERK^{f/f}$ DAT-Cre *vs.* WT DAT-Cre mice. For *de novo* protein synthesis in DA neurons detection the *n* refers to the number of mice per group (average of 40 somas per slice, 2 slices per mouse, from three independent experiments). All cell counting experiments were conducted blind to experimental group. All images were subsequently processed using ImageJ (NIH, USA).

Protein synthesis assay.

Proteins were labeled using a protocol adapted from the SUnSET method[107]. Briefly, 400 μm-thick brain slices containing SNc and VTA from 3-month old $eIF2\alpha^{(S51A/S51A)}$ DAT-Cre mice and control mice were prepared using a vibratome. Slices were allowed to recover in artificial cerebral spinal fluid (ACSF) at 32°C for 1 hour and subsequently treated with puromycin (P8833, Sigma-Aldrich, 5μg/mL) for 45 mins. Newly synthesized proteins were end-labeled with puromycin. SNc and VTA were micro-dissected from the brain slices and flash frozen on dry ice. Protein lysates were prepared for western blotting. Protein synthesis levels were determined by taking total lane density in the molecular weight range of 10 kDa to 250 kDa. Comparisons of protein synthesis levels between both genotypes were made by normalizing to the average WT DAT-Cre signal.

Thapsigargin-induced ER stress assay.

To induce ER stress, 400 μm-thick brain slices containing SNc and VTA from 3-month old mice were allowed to recover in ACSF at 32°C for 1 hr and subsequently treated with 1 μM Thapsigargin (Sigma-Aldrich, cat no: T9033) at 32°C for 2 hrs. ER stress was measured using either western blotting or immunofluorescent staining to detect PERK, p-eIF2α and ATF4 levels. SNc and VTA were punched out from the brain slices and processed by western blotting, whereas slices processed for immunofluorescence were embedded in 3% agarose solution and re-sliced at 40-μm thickness using a vibratome (Leica VT1200S; Leica Microsystems; Bannockburn, IL).

Western blotting.

SNc and VTA were separately micro-dissected from the brain slices and sonicated in ice-cold homogenization buffer (10 mM HEPES, 150 mM NaCl, 50 mM NaF, 1 mM EDTA, 1 mM EGTA, 10 mM Na4P2O7, 1% Triton X-100, 0.1% SDS and 10% glycerol) that was freshly supplemented with HALT protease and phosphatase inhibitor cocktail (Thermo Scientific, cat no: 78441, 1/10 total volume). Aliquots (2 μl) of the homogenate were used for protein determination with a BCA (bicinchoninic acid) assay kit (GE Healthcare). Samples were prepared with 5X sample buffer (0.25 M Tris-HCl pH6.8, 10%

SDS, 0.05% bromophenol blue, 50% glycerol and 25% - β mercaptoethanol) and heat denatured at 95ºC for 5 min. 40 μg protein per lane was run in pre-cast 4–12% Bis-Tris gels (Invitrogen) and subjected to SDS-PAGE followed by wet gel transfer to polyvinylidene difluoride (PVDF; Immobilon-Psq, Millipore Corporation, Billerica, USA) membranes. The membranes were probed overnight at 4°C using primary antibodies against p-eIF2α S51 (rabbit, Cell Signaling cat no: 9721, 1:500), anti-t-eIF2α (rabbit, Cell Signaling, cat no: 9722, 1:500), anti-puromycin (mouse, Millipore, cat no: MABE343, 1:1000). An antibody against β tubulin (mouse, Sigma, cat no: T8328, 1:1000) was used to estimate the total amount of protein. The membranes were probed with horseradish peroxidase-conjugated secondary IgG (1:7000, Promega) for 1 hr at room temperature. Signals from membranes were detected with ECL chemiluminescence (GE Healthcare Amersham™) using Alpha Imager 3.4 software and the FluorChem Protein Simple instrument. Exposures were set to obtain signals at the linear range and then normalized by total protein and quantified via densitometry using ImageJ software (NIH, USA).

Electrophysiology.

Striatal and hippocampal slice preparation and the recording of extracellular field excitatory postsynaptic potentials (fEPSPs) were performed as described previously[104]. Briefly, striatal and hippocampal slices from mice 3 to 4 months of age were isolated and transferred to recording chambers (preheated to 32 °C), where they were superfused with oxygenated artificial cerebrospinal fluid (ACSF). In all experiments, basal fEPSPs were stable for at least 20 min before the start of each experiment, and all slices recovered in the recording chamber at least 1 hr before recordings began. Briefly, three trains of high-frequency stimulation (3 sec duration, 100 Hz frequency at 20 sec intervals) were used to induced LTD in striatal slices, while hippocampal L-LTP was induced with three 1 s 100-Hz high-frequency stimulation trains, with an intertrain interval of 60 sec[108]. After induction of either striatal LTD or hippocampal L-LTP, fEPSPs were collected for an additional 70 min and 140 min, respectively. Slope values of fEPSP were expressed as a percent of the baseline average before LTD or L-LTP induction.

Voltammetric monitoring of DA release using FSCV.

Mice were deeply anesthetized with isoflurane, decapitated and brains were sliced with a Leica VT1200S vibratome (Leica Microsystems; Bannockburn, IL). Coronal forebrain slices (300 μm thickness) were cut in an ice cold HEPES-buffered artificial cerebrospinal fluid (aCSF) that contained (in mM): NaCl (120), $NaHCO_3$ (20), glucose (10), HEPES acid (6.7), KCl (5), HEPES sodium salt (3.3), $CaCl_2$ (2), and $MgSO_4$ (2), bubbled with a 95% O_2/5% CO_2 gas mixture and recovered in this solution for 1 h at room temperature prior to recordings. Slices were transferred to the recording chamber, maintained at 32 °C and superfused (1.5 mL/min) with aCSF that contained (in mM): NaCl (124), KCl (3.7), $NaHCO_3$ (26), $CaCl_2$ (2.4), $MgSO_4$ (1.3), KH_2PO_4 (1.3), glucose (10) equilibrated with 95% O_2/5% CO_2. Recordings were started after 30 min stabilization in the chamber. A Millar Voltammeter (available from Dr. Julian Millar, University of London, UK) was used for FSCV detection of evoked increased in $[DA]_o$, as described previously[1,109]. Locally evoked DA release was detected using carbon fiber microelectrodes, constructed in house from 7-μm diameter carbon fibers (Goodfellow Corporation, Berwyn, PA, USA), with 30–70

μm exposed length. For FSCV, a triangular voltage ramp (from −0.7 to +1.3 V, then back to −0.7 V *vs.* Ag/AgCl) was applied every 100 ms at a scan rate of 800 V/s. Increases in $[DA]_o$ in CPu and NAc core and shell were evoked using a concentric stimulating electrode positioned within 100 μm of the recording site. Single-pulse stimulation (400 μA, 0.1 ms duration) was used in CPu and NAc core, and a brief high-frequency pulse train (5 pulses at 100 Hz) was used in NAc shell to amplify evoked DA release. The currents resulting from DA oxidation were converted to DA concentration according to calibration with known concentrations of DA. To compare DA release in slices from control and $PERK^{f/f}$ DAT-Cre or $PERK^{f/f}$ TH-Cre mice, DA release was evoked in 4–5 sites in each striatal subregion in two slices per mouse. In all experiments after initial sampling under control conditions, a nAChR antagonist, DHβE (1 μM) was applied. A maximal drug effect was seen within 15 min, and multiple site sampling was repeated.

DAT-mediated dopamine uptake analysis.

The evaluation of changes in DAT activity was done using a MATLAB® script. C_{peak} values (peak concentration) and V_{max} values (maximum uptake velocity) for DAT-mediated dopamine uptake, derived from Michaelis-Menten analysis of single pulse evoked $[DA]_o$ records, were determined as described previously[110]using a fixed K_m of 0.9 μM[111] for each brain region and genotype. Data from the CPu and NAc core were used for this analysis because it was developed to extract uptake terms from $[DA]_o$ transients evoked by single-pulse stimulation, which was used in these regions. It should be noted that all mice were heterozygous DAT-cre, which exhibit a small but significant impairment in DAT function[112].

HPLC analysis of striatal DA content.

Quantification of DA content in experimental striatal slices was performed using HPLC with electrochemical detection, as described previously[109]. The dorsal and ventral striatum were dissected from each slice, with careful removal of overlying cortex and white matter. Samples (3–7 mg) were weighed, then frozen immediately on dry ice and stored at −80° C until processing. On the day of analysis, samples were diluted 1:10 in ice-cold mobile phase deoxygenated with argon, sonicated, centrifuged at 13,000 x g for 2 min and then the supernatant injected onto the HPLC.

Statistical analysis.

All data are presented as the mean ± SEM. Data was analyzed using GraphPad Prism 8. For behavioral experiments the experimenter was blinded to the genotype of the animals during behavioral testing. For two-group comparisons, statistical significance was determined by parametric and nonparametric two-tailed Student's t tests. Multi-groups were analyzed using one-way ANOVA or two-way ANOVA. P values less than 0.05 were considered statistically significant. Extreme outliers were detected by applying Grubbs' method with $\alpha = 0.05$ to each experimental group and eliminated from further analysis (GraphPad software). Sample size was chosen following previous publications. Data distribution was assessed to be normal. Variance was similar between the groups that were being statistically compared based on our observation. For voltammetry experiments and C_{peak}/V_{max} analysis *n* represents the number of recorded sites sampled from 3 to 5 mice per genotype.

Statistically significant differences measured for WT *vs.* KO were assessed with two-tailed unpaired *t*-test with Welch's correction for unequal variance in 3-month-old mice during the C_{peak}/V_{max} analysis. For this latter, values with $R^2 < 0.95$ indicating goodness-of-fit were excluded from the data reported here. For the HPLC analysis, *n* is the number of samples analyzed for each region, with two to six samples per animal. Significance of differences was calculated using unpaired Student's *t*-test. Statistical significance was considered to be $P < 0.05$.

Data availability.

The data that support the findings of this study are available from the corresponding author upon request.

Supplementary Material

Refer to Web version on PubMed Central for supplementary material.

Acknowledgement

We thank Dr. Caroline Bass (University at Buffalo) for providing the AAV2/10-TH-iCre and AAV2/10-TH-dsRED adeno-associated viruses and Dr. Randal Kaufman (Sanford Burnham Prebys Medical Discovery Institute) for providing the Eif2(S51A) mouse line; We wish to acknowledge Claudia Farb for exceptional technical assistance and Dr. Prerana Shrestha for critical advice and review of this manuscript. We thank all members of the Klann laboratory for critical feedback and discussions. The MATLAB script for Vmax analysis was written and provided by Dr. Charles Nicholson at NYU Grossman School of Medicine. This study was supported by National Institutes of Health Grants NS034007 and NS047384 (E.K.), DA038616 (M.E.R.), U.S. Department of Defense Award W81XWH-15-1-0360 (E.K.), and the Marlene and Paolo Fresco Institute for Parkinson's Disease and Movement Disorders (M.M. and M.E.R.).

References

1. Costa-Mattioli M, Gobert D, Stern E, Gamache K, Colina R, Cuello C et al. eIF2α phosphorylation bidirectionally regulates the switch from short-to long-term synaptic plasticity and memory. Cell 2007;129: 195–206. [PubMed: 17418795]
2. Di Prisco GV, Huang W, Buffington SA, Hsu C-C, Bonnen PE, Placzek AN et al. Translational control of mGluR-dependent long-term depression and object-place learning by eIF2α. Nature neuroscience 2014;17: 1073–1082. [PubMed: 24974795]
3. Trinh MA & Klann E Translational control by eIF2α kinases in long-lasting synaptic plasticity and long-term memory. Neurobiology of learning and memory 2013;105: 93–99. [PubMed: 23707798]
4. Ma T, Trinh MA, Wexler AJ, Bourbon C, Gatti E, Pierre P et al. Suppression of eIF2α kinases alleviates Alzheimer's disease–related plasticity and memory deficits. Nature neuroscience 2013;16: 1299. [PubMed: 23933749]
5. Trinh MA, Kaphzan H, Wek RC, Pierre P, Cavener DR & Klann E Brain-specific disruption of the eIF2α kinase PERK decreases ATF4 expression and impairs behavioral flexibility. Cell reports 2012;1: 676–688. [PubMed: 22813743]
6. Trinh MA, Ma T, Kaphzan H, Bhattacharya A, Antion MD, Cavener DR et al. The eIF2α kinase PERK limits the expression of hippocampal metabotropic glutamate receptor-dependent long-term depression. Learning & memory 2014;21: 298–304. [PubMed: 24741110]
7. Zhu PJ, Huang W, Kalikulov D, Yoo JW, Placzek AN, Stoica L et al. Suppression of PKR promotes network excitability and enhanced cognition by interferon-γ-mediated disinhibition. Cell 2011;147: 1384–1396. [PubMed: 22153080]
8. Stern E, Chinnakkaruppan A, David O, Sonenberg N & Rosenblum K Blocking the eIF2α kinase (PKR) enhances positive and negative forms of cortex-dependent taste memory. Journal of Neuroscience 2013;33: 2517–2525. [PubMed: 23392680]

9. Ounallah-Saad H, Sharma V, Edry E & Rosenblum K Genetic or pharmacological reduction of PERK enhances cortical-dependent taste learning. Journal of Neuroscience 2014;34: 14624–14632. [PubMed: 25355215]
10. Sharma V, Ounallah-Saad H, Chakraborty D, Hleihil M, Sood R, Barrera I et al. Local inhibition of PERK enhances memory and reverses age-related deterioration of cognitive and neuronal properties. Journal of Neuroscience 2018;38: 648–658. [PubMed: 29196323]
11. Yang W, Zhou X, Zimmermann HR & Ma T Brain-specific suppression of AMPKα2 isoform impairs cognition and hippocampal LTP by PERK-mediated eIF2α phosphorylation. Molecular Psychiatry 2020: 1–18.
12. Ellgaard L & Helenius A Quality control in the endoplasmic reticulum. Nature reviews Molecular cell biology 2003;4: 181. [PubMed: 12612637]
13. Martínez G, Duran-Aniotz C, Cabral-Miranda F, Vivar JP & Hetz C Endoplasmic reticulum proteostasis impairment in aging. Aging Cell 2017;16: 615–623. [PubMed: 28436203]
14. Hetz C The unfolded protein response: controlling cell fate decisions under ER stress and beyond. Nature reviews Molecular cell biology 2012;13: 89–102. [PubMed: 22251901]
15. Hetz C & Mollereau B Disturbance of endoplasmic reticulum proteostasis in neurodegenerative diseases. Nature Reviews Neuroscience 2014;15: 233. [PubMed: 24619348]
16. Hughes D & Mallucci GR The unfolded protein response in neurodegenerative disorders–therapeutic modulation of the PERK pathway. The FEBS journal 2018
17. Smith HL & Mallucci GR The unfolded protein response: mechanisms and therapy of neurodegeneration. Brain 2016;139: 2113–2121. [PubMed: 27190028]
18. Scheper W & Hoozemans JJ The unfolded protein response in neurodegenerative diseases: a neuropathological perspective. Acta neuropathologica 2015;130: 315–331. [PubMed: 26210990]
19. Gold PW, Licinio J & Pavlatou M Pathological parainflammation and endoplasmic reticulum stress in depression: potential translational targets through the CNS insulin, klotho and PPAR-γ systems. Molecular psychiatry 2013;18: 154–165. [PubMed: 23183489]
20. So J, Warsh JJ & Li PP Impaired endoplasmic reticulum stress response in B-lymphoblasts from patients with bipolar-I disorder. Biological psychiatry 2007;62: 141–147. [PubMed: 17217928]
21. Kim P, Scott MR & Meador-Woodruff JH Dysregulation of the unfolded protein response (UPR) in the dorsolateral prefrontal cortex in elderly patients with schizophrenia. Molecular Psychiatry 2019: 1–11.
22. Walter P & Ron D The unfolded protein response: from stress pathway to homeostatic regulation. Science 2011;334: 1081–1086. [PubMed: 22116877]
23. Klann E & Dever TE Biochemical mechanisms for translational regulation in synaptic plasticity. Nature Reviews Neuroscience 2004;5: 931. [PubMed: 15550948]
24. Urra H, Dufey E, Lisbona F, Rojas-Rivera D & Hetz C When ER stress reaches a dead end. Biochimica et Biophysica Acta (BBA)-Molecular Cell Research 2013;1833: 3507–3517. [PubMed: 23988738]
25. Aguzzi A & O'connor T Protein aggregation diseases: pathogenicity and therapeutic perspectives. Nature reviews Drug discovery 2010;9: 237. [PubMed: 20190788]
26. Bandopadhyay R & de Belleroche J Pathogenesis of Parkinson's disease: emerging role of molecular chaperones. Trends in molecular medicine 2010;16: 27–36. [PubMed: 20036196]
27. Soto C Unfolding the role of protein misfolding in neurodegenerative diseases. Nature Reviews Neuroscience 2003;4: 49. [PubMed: 12511861]
28. Hoozemans JJ, Van Haastert ES, Nijholt DA, Rozemuller AJ & Scheper W Activation of the unfolded protein response is an early event in Alzheimer's and Parkinson's disease. Neurodegenerative Diseases 2012;10: 212–215. [PubMed: 22302012]
29. Saxena S & Caroni P Selective neuronal vulnerability in neurodegenerative diseases: from stressor thresholds to degeneration. Neuron 2011;71: 35–48. [PubMed: 21745636]
30. Mercado G, Castillo V, Soto P, López N, Axten JM, Sardi SP et al. Targeting PERK signaling with the small molecule GSK2606414 prevents neurodegeneration in a model of Parkinson's disease. Neurobiology of disease 2018;112: 136–148. [PubMed: 29355603]

31. Schicknick H, Schott BH, Budinger E, Smalla K-H, Riedel A, Seidenbecher CI et al. Dopaminergic modulation of auditory cortex-dependent memory consolidation through mTOR. Cerebral Cortex 2008;18: 2646–2658. [PubMed: 18321872]
32. Broussard JI, Yang K, Levine AT, Tsetsenis T, Jenson D, Cao F et al. Dopamine regulates aversive contextual learning and associated in vivo synaptic plasticity in the hippocampus. Cell reports 2016;14: 1930–1939. [PubMed: 26904943]
33. Rosen ZB, Cheung S & Siegelbaum SA Midbrain dopamine neurons bidirectionally regulate CA3-CA1 synaptic drive. Nature neuroscience 2015;18: 1763. [PubMed: 26523642]
34. Kesby J, Eyles D, McGrath J & Scott J Dopamine, psychosis and schizophrenia: the widening gap between basic and clinical neuroscience. Translational psychiatry 2018;8: 1–12. [PubMed: 29317594]
35. Volkow ND, Fowler JS, Wang G-J & Swanson JM Dopamine in drug abuse and addiction: results from imaging studies and treatment implications. Molecular psychiatry 2004;9: 557–569. [PubMed: 15098002]
36. Frank MJ, Santamaria A, O'Reilly RC & Willcutt E Testing computational models of dopamine and noradrenaline dysfunction in attention deficit/hyperactivity disorder. Neuropsychopharmacology 2007;32: 1583–1599. [PubMed: 17164816]
37. Denys D, van der Wee N, Janssen J, De Geus F & Westenberg HG Low level of dopaminergic D2 receptor binding in obsessive-compulsive disorder. Biological psychiatry 2004;55: 1041–1045. [PubMed: 15121489]
38. Maia TV & Conceição VA Dopaminergic disturbances in Tourette syndrome: an integrative account. Biological psychiatry 2018;84: 332–344. [PubMed: 29656800]
39. Hamilton PJ, Campbell NG, Sharma S, Erreger K, Hansen FH, Saunders C et al. De novo mutation in the dopamine transporter gene associates dopamine dysfunction with autism spectrum disorder. Molecular psychiatry 2013;18: 1315–1323. [PubMed: 23979605]
40. Ma T & Klann E PERK: a novel therapeutic target for neurodegenerative diseases? Alzheimer's research & therapy 2014;6: 30.
41. Moreno JA, Radford H, Peretti D, Steinert JR, Verity N, Martin MG et al. Sustained translational repression by eIF2α-P mediates prion neurodegeneration. Nature 2012;485: 507. [PubMed: 22622579]
42. Hetz C, Axten JM & Patterson JB Pharmacological targeting of the unfolded protein response for disease intervention. Nature chemical biology 2019;15: 764–775. [PubMed: 31320759]
43. Hetz C & Saxena S ER stress and the unfolded protein response in neurodegeneration. Nature Reviews Neurology 2017;13: 477. [PubMed: 28731040]
44. Bäckman CM, Malik N, Zhang Y, Shan L, Grinberg A, Hoffer BJ et al. Characterization of a mouse strain expressing Cre recombinase from the 3′ untranslated region of the dopamine transporter locus. genesis 2006;44: 383–390. [PubMed: 16865686]
45. Zhang P, McGrath B, Li S. a., Frank A, Zambito F, Reinert J et al. The PERK eukaryotic initiation factor 2α kinase is required for the development of the skeletal system, postnatal growth, and the function and viability of the pancreas. Molecular and cellular biology 2002;22: 3864–3874. [PubMed: 11997520]
46. Madisen L, Zwingman TA, Sunkin SM, Oh SW, Zariwala HA, Gu H et al. A robust and high-throughput Cre reporting and characterization system for the whole mouse brain. Nature neuroscience 2010;13: 133. [PubMed: 20023653]
47. Nobili A, Latagliata EC, Viscomi MT, Cavallucci V, Cutuli D, Giacovazzo G et al. Dopamine neuronal loss contributes to memory and reward dysfunction in a model of Alzheimer's disease. Nature communications 2017;8: 14727.
48. Scheuner D, Song B, McEwen E, Liu C, Laybutt R, Gillespie P et al. Translational control is required for the unfolded protein response and in vivo glucose homeostasis. Molecular cell 2001;7: 1165–1176. [PubMed: 11430820]
49. Tritsch NX & Sabatini BL Dopaminergic modulation of synaptic transmission in cortex and striatum. Neuron 2012;76: 33–50. [PubMed: 23040805]

50. Chen JY, Wang EA, Cepeda C & Levine MS Dopamine imbalance in Huntington's disease: a mechanism for the lack of behavioral flexibility. Frontiers in neuroscience 2013;7: 114. [PubMed: 23847463]
51. Howes OD, Montgomery AJ, Asselin M-C, Murray RM, Valli I, Tabraham P et al. Elevated striatal dopamine function linked to prodromal signs of schizophrenia. Archives of general psychiatry 2009;66: 13–20. [PubMed: 19124684]
52. Egerton A, Chaddock CA, Winton-Brown TT, Bloomfield MA, Bhattacharyya S, Allen P et al. Presynaptic striatal dopamine dysfunction in people at ultra-high risk for psychosis: findings in a second cohort. Biological psychiatry 2013;74: 106–112. [PubMed: 23312565]
53. Cousins DA, Butts K & Young AH The role of dopamine in bipolar disorder. Bipolar disorders 2009;11: 787–806. [PubMed: 19922550]
54. Nieminen-von Wendt TS, Metsähonkala L, Kulomäki TA, Aalto S, Autti TH, Vanhala R et al. Increased presynaptic dopamine function in Asperger syndrome. Neuroreport 2004;15: 757–760. [PubMed: 15073509]
55. Björklund A & Dunnett SB Dopamine neuron systems in the brain: an update. Trends in neurosciences 2007;30: 194–202. [PubMed: 17408759]
56. Zhou F-M, Liang Y & Dani JA Endogenous nicotinic cholinergic activity regulates dopamine release in the striatum. Nature neuroscience 2001;4: 1224. [PubMed: 11713470]
57. Rice ME & Cragg SJ Nicotine amplifies reward-related dopamine signals in striatum. Nature neuroscience 2004;7: 583. [PubMed: 15146188]
58. Cachope R, Mateo Y, Mathur BN, Irving J, Wang H-L, Morales M et al. Selective activation of cholinergic interneurons enhances accumbal phasic dopamine release: setting the tone for reward processing. Cell reports 2012;2: 33–41. [PubMed: 22840394]
59. Threlfell S, Lalic T, Platt NJ, Jennings KA, Deisseroth K & Cragg SJ Striatal dopamine release is triggered by synchronized activity in cholinergic interneurons. Neuron 2012;75: 58–64. [PubMed: 22794260]
60. Viaro R, Calcagno M, Marti M, Borrelli E & Morari M Pharmacological and genetic evidence for pre-and postsynaptic D2 receptor involvement in motor responses to nociceptin/orphanin FQ receptor ligands. Neuropharmacology 2013;72: 126–138. [PubMed: 23643745]
61. Calabresi P, Saiardi A, Pisani A, Baik J-H, Centonze D, Mercuri NB et al. Abnormal synaptic plasticity in the striatum of mice lacking dopamine D2 receptors. Journal of Neuroscience 1997;17: 4536–4544. [PubMed: 9169514]
62. Yin HH, Davis MI, Ronesi JA & Lovinger DM The role of protein synthesis in striatal long-term depression. Journal of Neuroscience 2006;26: 11811–11820. [PubMed: 17108154]
63. Lüscher C & Huber KM Group 1 mGluR-dependent synaptic long-term depression: mechanisms and implications for circuitry and disease. Neuron 2010;65: 445–459. [PubMed: 20188650]
64. Calabresi P, Picconi B, Tozzi A & Di Filippo M Dopamine-mediated regulation of corticostriatal synaptic plasticity. Trends in neurosciences 2007;30: 211–219. [PubMed: 17367873]
65. Goldberg MS, Pisani A, Haburcak M, Vortherms TA, Kitada T, Costa C et al. Nigrostriatal dopaminergic deficits and hypokinesia caused by inactivation of the familial Parkinsonism-linked gene DJ-1. Neuron 2005;45: 489–496. [PubMed: 15721235]
66. Russo SJ & Nestler EJ The brain reward circuitry in mood disorders. Nature Reviews Neuroscience 2013;14: 609–625. [PubMed: 23942470]
67. Gompf HS, Budygin EA, Fuller PM & Bass CE Targeted genetic manipulations of neuronal subtypes using promoter-specific combinatorial AAVs in wild-type animals. Frontiers in behavioral neuroscience 2015;9: 152. [PubMed: 26190981]
68. Edwards NJ, Tejeda HA, Pignatelli M, Zhang S, McDevitt RA, Wu J et al. Circuit specificity in the inhibitory architecture of the VTA regulates cocaine-induced behavior. Nature neuroscience 2017;20: 438. [PubMed: 28114294]
69. Lee HJ, Gallagher M & Holland PC The central amygdala projection to the substantia nigra reflects prediction error information in appetitive conditioning. Learning & Memory 2010;17: 531–538. [PubMed: 20889725]

70. Duran-Aniotz C, Cornejo VH, Espinoza S, Ardiles ÁO, Medinas DB, Salazar C et al. IRE1 signaling exacerbates Alzheimer's disease pathogenesis. Acta neuropathologica 2017;134: 489–506. [PubMed: 28341998]
71. Cooper AA, Gitler AD, Cashikar A, Haynes CM, Hill KJ, Bhullar B et al. α-Synuclein blocks ER-Golgi traffic and Rab1 rescues neuron loss in Parkinson's models. Science 2006;313: 324–328. [PubMed: 16794039]
72. Costa-Mattioli M, Gobert D, Harding H, Herdy B, Azzi M, Bruno M et al. Translational control of hippocampal synaptic plasticity and memory by the eIF2α kinase GCN2. Nature 2005;436: 1166. [PubMed: 16121183]
73. Jiang Z, Belforte JE, Lu Y, Yabe Y, Pickel J, Smith CB et al. eIF2α phosphorylation-dependent translation in CA1 pyramidal cells impairs hippocampal memory consolidation without affecting general translation. Journal of Neuroscience 2010;30: 2582–2594. [PubMed: 20164343]
74. Sidrauski C, Acosta-Alvear D, Khoutorsky A, Vedantham P, Hearn BR, Li H et al. Pharmacological brake-release of mRNA translation enhances cognitive memory. Elife 2013;2: e00498. [PubMed: 23741617]
75. Tsaytler P, Harding HP, Ron D & Bertolotti A Selective inhibition of a regulatory subunit of protein phosphatase 1 restores proteostasis. Science 2011;332: 91–94. [PubMed: 21385720]
76. Bond S, Lopez-Lloreda C, Gannon PJ, Akay-Espinoza C & Jordan-Sciutto KL The Integrated Stress Response and Phosphorylated Eukaryotic Initiation Factor 2α in Neurodegeneration. Journal of Neuropathology & Experimental Neurology 2020
77. Rittiner JE, Caffall ZF, Hernández-Martinez R, Sanderson SM, Pearson JL, Tsukayama KK et al. Functional genomic analyses of mendelian and sporadic disease identify impaired eIF2α signaling as a generalizable mechanism for dystonia. Neuron 2016;92: 1238–1251. [PubMed: 27939583]
78. Kabir Z, Che A, Fischer D, Rice R, Rizzo B, Byrne M et al. Rescue of impaired sociability and anxiety-like behavior in adult cacna1c-deficient mice by pharmacologically targeting eIF2α. Molecular psychiatry 2017;22: 1096–1109. [PubMed: 28584287]
79. Arioka Y, Shishido E, Kushima I, Suzuki T, Saito R, Aiba A et al. Chromosome 22q11. 2 deletion causes PERK-dependent vulnerability in dopaminergic neurons. EBioMedicine 2021;63: 103138. [PubMed: 33341442]
80. Buffington SA, Huang W & Costa-Mattioli M Translational control in synaptic plasticity and cognitive dysfunction. Annual review of neuroscience 2014;37: 17–38.
81. Brichta L & Greengard P Molecular determinants of selective dopaminergic vulnerability in Parkinson's disease: an update. Frontiers in neuroanatomy 2014;8: 152. [PubMed: 25565977]
82. Liljeholm M & O'Doherty JP Contributions of the striatum to learning, motivation, and performance: an associative account. Trends in cognitive sciences 2012;16: 467–475. [PubMed: 22890090]
83. Kreitzer AC & Malenka RC Endocannabinoid-mediated rescue of striatal LTD and motor deficits in Parkinson's disease models. Nature 2007;445: 643–647. [PubMed: 17287809]
84. Shen W, Flajolet M, Greengard P & Surmeier DJ Dichotomous dopaminergic control of striatal synaptic plasticity. Science 2008;321: 848–851. [PubMed: 18687967]
85. Grimm CM, Aksamaz S, Schulz S, Teutsch J, Sicinski P, Liss B et al. Schizophrenia-related cognitive dysfunction in the Cyclin-D2 knockout mouse model of ventral hippocampal hyperactivity. Translational psychiatry 2018;8: 1–16. [PubMed: 29317594]
86. Haber SN, Fudge JL & McFarland NR Striatonigrostriatal pathways in primates form an ascending spiral from the shell to the dorsolateral striatum. Journal of Neuroscience 2000;20: 2369–2382. [PubMed: 10704511]
87. Yang K & Dani JA Dopamine D1 and D5 receptors modulate spike timing-dependent plasticity at medial perforant path to dentate granule cell synapses. Journal of Neuroscience 2014;34: 15888–15897. [PubMed: 25429131]
88. Lemon N & Manahan-Vaughan D Dopamine D1/D5 receptors gate the acquisition of novel information through hippocampal long-term potentiation and long-term depression. Journal of Neuroscience 2006;26: 7723–7729. [PubMed: 16855100]

89. Swant J & Wagner JJ Dopamine transporter blockade increases LTP in the CA1 region of the rat hippocampus via activation of the D3 dopamine receptor. Learning & Memory 2006;13: 161–167. [PubMed: 16585791]

90. McNamara CG, Tejero-Cantero Á, Trouche S, Campo-Urriza N & Dupret D Dopaminergic neurons promote hippocampal reactivation and spatial memory persistence. Nature neuroscience 2014;17: 1658. [PubMed: 25326690]

91. Li S, Cullen WK, Anwyl R & Rowan MJ Dopamine-dependent facilitation of LTP induction in hippocampal CA1 by exposure to spatial novelty. Nature neuroscience 2003;6: 526. [PubMed: 12704392]

92. Hagena H & Manahan-Vaughan D Dopamine D1/D5, but not D2/D3, receptor dependency of synaptic plasticity at hippocampal mossy fiber synapses that is enabled by patterned afferent stimulation, or spatial learning. Frontiers in synaptic neuroscience 2016;8: 31. [PubMed: 27721791]

93. Guzmán-Ramos K, Moreno-Castilla P, Castro-Cruz M, McGaugh JL, Martínez-Coria H, LaFerla FM et al. Restoration of dopamine release deficits during object recognition memory acquisition attenuates cognitive impairment in a triple transgenic mice model of Alzheimer's disease. Learning & memory 2012;19: 453–460. [PubMed: 22984283]

94. Rossato JI, Radiske A, Kohler CA, Gonzalez C, Bevilaqua LR, Medina JH et al. Consolidation of object recognition memory requires simultaneous activation of dopamine D1/D5 receptors in the amygdala and medial prefrontal cortex but not in the hippocampus. Neurobiology of learning and memory 2013;106: 66–70. [PubMed: 23891712]

95. Maia TV & Frank MJ From reinforcement learning models to psychiatric and neurological disorders. Nature neuroscience 2011;14: 154. [PubMed: 21270784]

96. Lisman JE, Pi HJ, Zhang Y & Otmakhova NA A thalamo-hippocampal-ventral tegmental area loop may produce the positive feedback that underlies the psychotic break in schizophrenia. Biological psychiatry 2010;68: 17–24. [PubMed: 20553749]

97. Colla E, Jensen PH, Pletnikova O, Troncoso JC, Glabe C & Lee MK Accumulation of toxic α-synuclein oligomer within endoplasmic reticulum occurs in α-synucleinopathy in vivo. Journal of Neuroscience 2012;32: 3301–3305. [PubMed: 22399752]

98. Das I, Krzyzosiak A, Schneider K, Wrabetz L, D'Antonio M, Barry N et al. Preventing proteostasis diseases by selective inhibition of a phosphatase regulatory subunit. Science 2015;348: 239–242. [PubMed: 25859045]

99. Wang L, Popko B, Tixier E & Roos RP Guanabenz, which enhances the unfolded protein response, ameliorates mutant SOD1-induced amyotrophic lateral sclerosis. Neurobiology of disease 2014;71: 317–324. [PubMed: 25134731]

100. Back SH, Scheuner D, Han J, Song B, Ribick M, Wang J et al. Translation attenuation through eIF2α phosphorylation prevents oxidative stress and maintains the differentiated state in β cells. Cell metabolism 2009;10: 13–26. [PubMed: 19583950]

101. Longo F, Russo I, Shimshek DR, Greggio E & Morari M Genetic and pharmacological evidence that G2019S LRRK2 confers a hyperkinetic phenotype, resistant to motor decline associated with aging. Neurobiol Dis 2014;71: 62–73. [PubMed: 25107341]

102. Bhattacharya A, Kaphzan H, Alvarez-Dieppa AC, Murphy JP, Pierre P & Klann E Genetic removal of p70 S6 kinase 1 corrects molecular, synaptic, and behavioral phenotypes in fragile X syndrome mice. Neuron 2012;76: 325–337. [PubMed: 23083736]

103. Errico F, Santini E, Migliarini S, Borgkvist A, Centonze D, Nasti V et al. The GTP-binding protein Rhes modulates dopamine signalling in striatal medium spiny neurons. Mol Cell Neurosci 2008;37: 335–345. [PubMed: 18035555]

104. Santini E, Huynh TN, MacAskill AF, Carter AG, Pierre P, Ruggero D et al. Exaggerated translation causes synaptic and behavioural aberrations associated with autism. Nature 2013;493: 411–415. [PubMed: 23263185]

105. Huynh TN, Santini E & Klann E Requirement of Mammalian target of rapamycin complex 1 downstream effectors in cued fear memory reconsolidation and its persistence. J Neurosci 2014;34: 9034–9039. [PubMed: 24990923]

106. Bowling H, Bhattacharya A, Zhang G, Lebowitz JZ, Alam D, Smith PT et al. BONLAC: A combinatorial proteomic technique to measure stimulus-induced translational profiles in brain slices. Neuropharmacology 2016;100: 76–89. [PubMed: 26205778]

107. Schmidt EK, Clavarino G, Ceppi M & Pierre P SUnSET, a nonradioactive method to monitor protein synthesis. Nature methods 2009;6: 275. [PubMed: 19305406]

108. Hou L, Antion MD, Hu D, Spencer CM, Paylor R & Klann E Dynamic translational and proteasomal regulation of fragile X mental retardation protein controls mGluR-dependent long-term depression. Neuron 2006;51: 441–454. [PubMed: 16908410]

109. Stouffer MA, Woods CA, Patel JC, Lee CR, Witkovsky P, Bao L et al. Insulin enhances striatal dopamine release by activating cholinergic interneurons and thereby signals reward. Nature communications 2015;6: 8543.

110. Li X, Patel JC, Wang J, Avshalumov MV, Nicholson C, Buxbaum JD et al. Enhanced striatal dopamine transmission and motor performance with LRRK2 overexpression in mice is eliminated by familial Parkinson's disease mutation G2019S. Journal of Neuroscience 2010;30: 1788–1797. [PubMed: 20130188]

111. Schmitz Y, Lee CJ, Schmauss C, Gonon F & Sulzer D Amphetamine distorts stimulation-dependent dopamine overflow: effects on D2 autoreceptors, transporters, and synaptic vesicle stores. Journal of Neuroscience 2001;21: 5916–5924. [PubMed: 11487614]

112. O'Neill B, Patel JC & Rice ME Characterization of optically and electrically evoked dopamine release in striatal slices from digenic knock-in mice with DAT-driven expression of channelrhodopsin. ACS chemical neuroscience 2017;8: 310–319. [PubMed: 28177213]

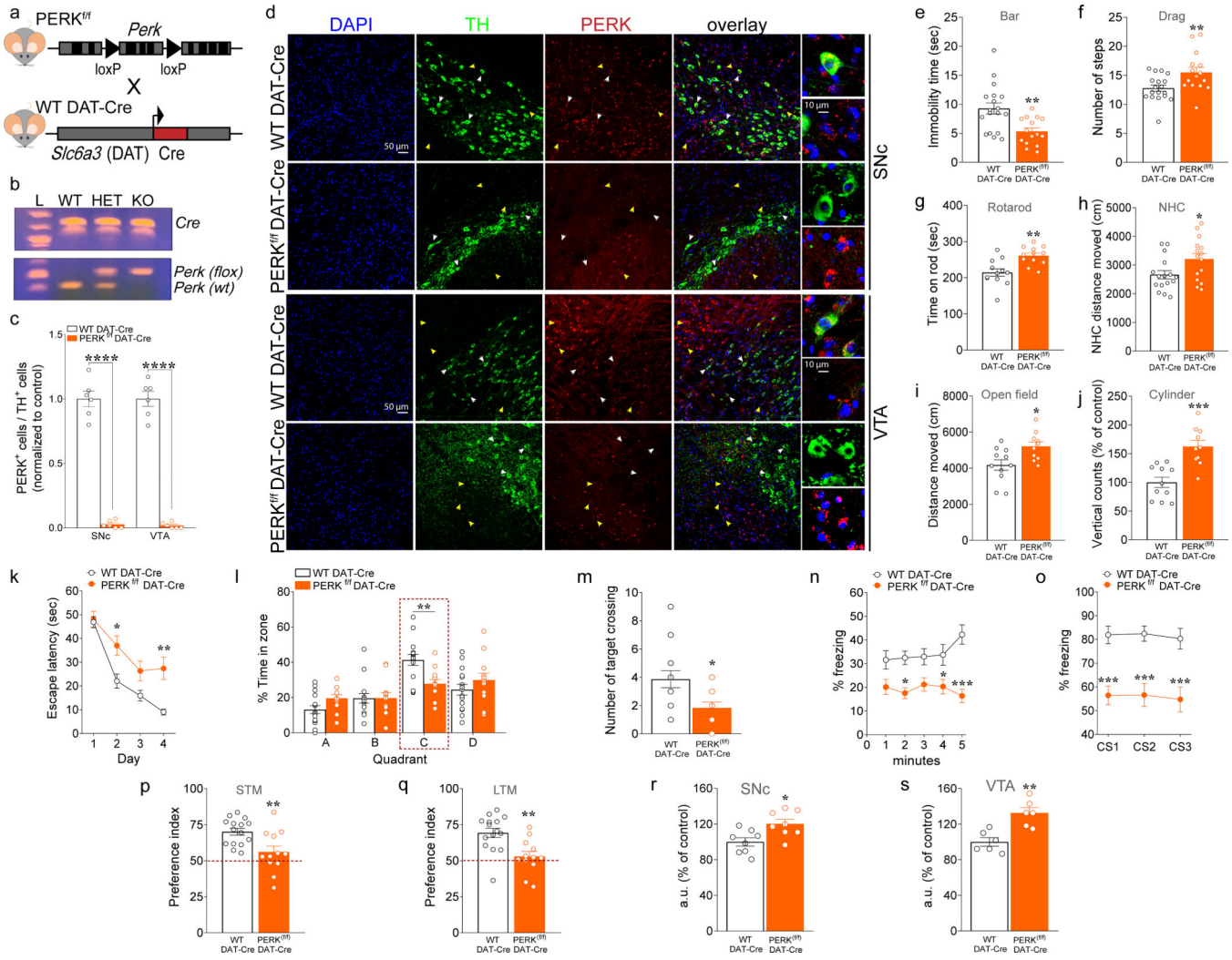

Figure 1. Deletion of PERK from DA neurons induces motor facilitation, but results in multiple cognitive phenotypes and dysregulated *de novo* translation in mice.

(**a**) Schematic representation of DAT-neuron specific deletion of PERK in PERK$^{f/f}$ mice crossed with WT DAT-Cre mice. (**b**) PCR identification of alleles of Perk^{loxP} and DAT-driven Cre. (**c**) Summary plot showing the ratio of TH+ cells in both the SNc and the VTA that co-labeled for PERK in PERK$^{f/f}$ DAT-Cre vs. WT DAT-Cre control mice (n = 6 mice each, unpaired *t* test, SNc: $t_{(10)}$= 15.85, P<0.0001; VTA: $t_{(10)}$= 16.86, P<0.0001) after treatment with thapsigargin. (**d**) Immunofluorescent detection of TH$^+$ (green) neurons and PERK (red) expression in SNc and VTA DA neurons of PERK$^{f/f}$ DAT-Cre and WT DAT-Cre mice, confirming positive targeting of dopaminergic (TH$^+$) neurons for the deletion of PERK (scale bars represent 50 µm). White arrows indicate dopaminergic neurons (green) and PERK (red) co-staining; yellow arrows indicate non-dopaminergic neurons and PERK (red) staining. PERK$^{f/f}$ DAT-Cre and their WT DAT-Cre littermates mice were subjected to a set of tests, including the bar (**e**), drag (**f**), rotarod (**g**), novel home cage (**h**), and open field (**i,j**) tests to investigate locomotor activity, at 3 months of age. (**e**) Summary plot of immobility time (sec) during bar test in PERK$^{f/f}$ DAT-Cre *versus* WT DAT-Cre mice (unpaired *t* test, $t_{(31)}$= 3.33, P<0.01). (**f**) Summary plot of average number of steps during

drag test (unpaired *t* test, $t_{(31)}$= 2.75, *P* <0.01). (**g**) Summary plot of latency to fall from the rotating rod measured as average of two days (4 trials/day) test (unpaired *t* test, $t_{(22)}$= 3.69, *P* <0.01). (**h**) Summary plot of the novelty-induced locomotor activity expressed as a novel home cage (NHC) distance moved (cm) in the first 10 minutes interval of a 60 minutes test during novel home cage test (unpaired *t* test, $t_{(29)}$= 2.31, *P* <0.05). (**i,j**) Summary plot of (**i**) spontaneous locomotor activity expressed as distance moved (cm) and (**j**) vertical activity (number of counts) during the open field test over 15 min (unpaired *t* test, **i**, $t_{(19)}$= 2.68, *P* <0.05; **j**, $t_{(19)}$= 4.56, *P* <0.001).

(**k**-**m**) Summary plots of (**k**) average latency to find the hidden platform during a 4-day training protocol, (**l**) percentage time spent in each zone, and (**o**) average number of times crossing the location of the previously hidden platform during probe test in 3- month old $PERK^{f/f}$ DAT-Cre *versus* WT DAT-Cre mice in the MWM test (**k**, two-way RM ANOVA, followed by Bonferroni's multiple comparisons test, time x genotype, $F_{(3, 75)}$ = 3.53, *P* < 0.05; **l**, two-way RM ANOVA, followed by Bonferroni's multiple comparisons test, quadrant x genotype, $F_{(3, 75)}$ = 3.77, *P* < 0.05; **m**, unpaired *t* test, $t_{(25)}$ = 2.607, *P* = 0.02). (**n,o**) Summary plots of average percentage of freezing during (**n**) exposure to the context 24 hours after training, and (**o**) exposure to 3 CS presentations in a novel context in the associative threat memory test in 3-month old $PERK^{f/f}$ DAT-Cre *versus* WT DAT-Cre mice (**n**, two-way RM ANOVA, followed by Bonferroni's multiple comparisons test, genotype, $F_{(1, 25)}$ = 20.45, *P* = 0.0001; **o**, two-way RM ANOVA, followed by Bonferroni's multiple comparisons test, genotype, $F_{(1, 25)}$ = 28.53 *P* <0.0001). (**p,q**) Summary plots of preference indices of mice towards a novel object introduced in the novel object recognition test in 3-month old $PERK^{f/f}$ DAT-Cre *versus* WT DAT-Cre mice (unpaired *t* test; **p**, $t_{(25)}$ = 3.079, *P* < 0.01; **q**, $t_{(25)}$ = 3.433, *P* < 0.01;). Mice were analyzed using Student's *t* test or two-way RM ANOVA, followed by Bonferroni's test for multiple comparisons. **P* < 0.05, ***P* < 0.01, ****P* < 0.001 different from age-matched littermates. All data are shown as mean ± s.e.m. of *n* = 15–18 mice/genotype (**e,f**); *n* = 12 mice/genotype (**g**); *n* = 15–16 mice/genotype (**h**); *n* = 10–11 mice/genotype (**i,j**); *n* = 12–15 mice/genotype (**k-q**). All data are shown as mean ± s.e.m. **P* < 0.05, ***P* < 0.01 and ****P* < 0.001 $PERK^{f/f}$ DAT-Cre *versus* WT DAT-Cre mice. (**r**,**s**) Quantification of increased AHA-alkyne-Alexa 647 signal in fluorescent arbitrary units (a.u.) expressed as % of control in TH+ neurons (Green) from SNc (**r**) and VTA (**s**) of $PERK^{f/f}$ DAT-Cre vs. WT DAT-Cre mice. Cell soma intensity was measured in ImageJ. Statistical significance was determined by using Student's *t* test ($PERK^{f/f}$ DAT-Cre vs. WT DAT-Cre mice; unpaired *t* test; **r**, $t_{(14)}$ = 2.933, *P* = 0.011; **s**, $t_{(10)}$ = 4.215, *P* = 0.002). Data are shown as mean ± s.e.m. of *n* = 6/8 mice per group (average of *n* = 40 somas per slice, *n* = 2 slices per mouse, from three independent experiments) **P* < 0.05, ***P* < 0.01.

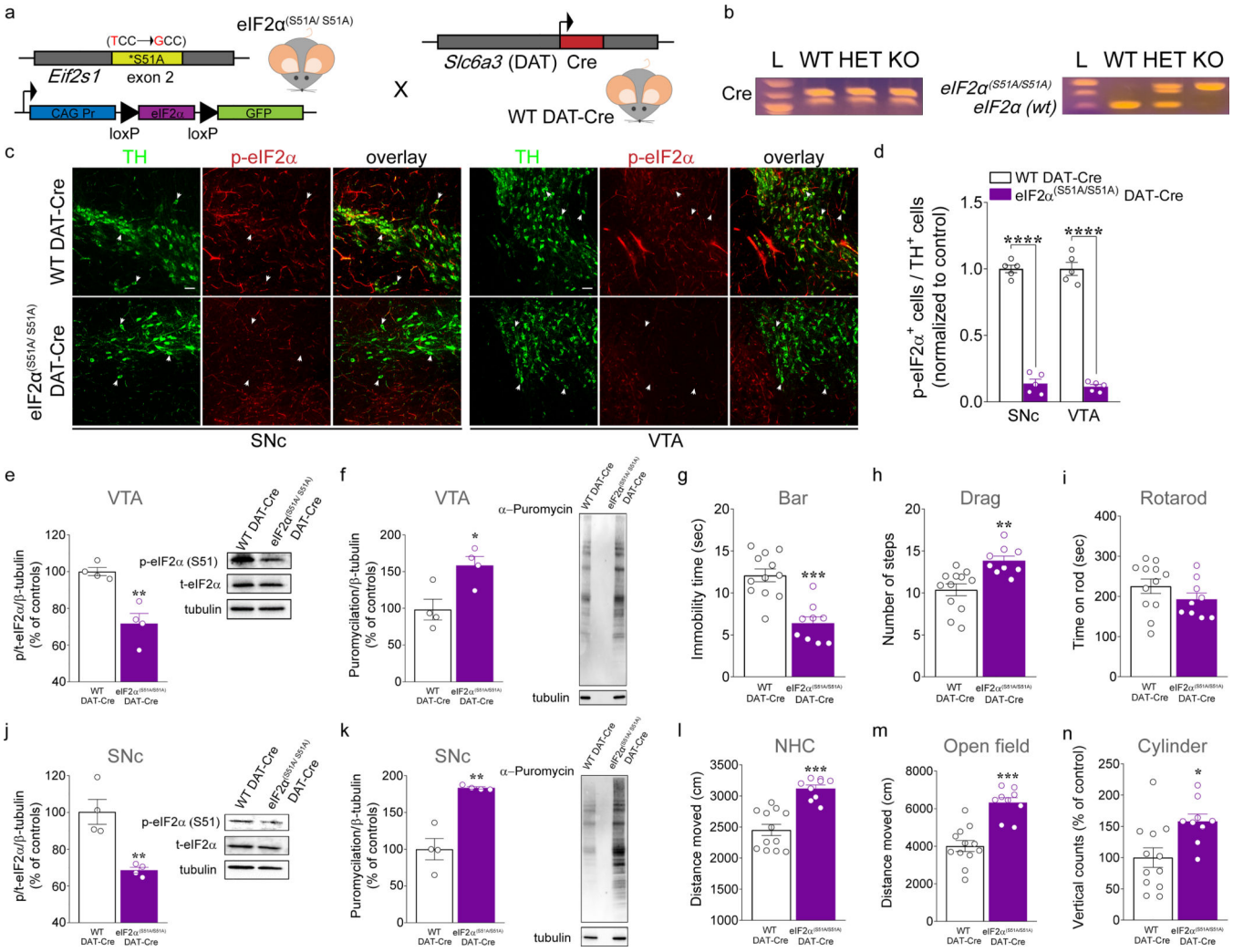

Figure 2. eIF2α$^{(S51A/S51A)}$ DAT-Cre mice display enhanced locomotor activity.

(**a**) Schematic representation of DAT-neuron specific expression of phospho-mutant eIF2α in eIF2α$^{(S51A/S51A)}$ mice crossed with WT DAT-Cre mice. (**b**) PCR identification of alleles of eIF2α$^{(S51A/S51A)}$ and DAT-driven Cre. (**c**) Immunofluorescent detection of TH^{+} (green) neurons and phospho-eIF2α (p-eIF2α; red) expression in SNc and VTA DA neurons of eIF2α$^{(S51A/S51A)}$ DAT-Cre and WT DAT-Cre mice, confirming positive targeting of dopaminergic (TH^{+}) neurons for the expression of phospho-mutant eIF2α (scale bars represent 50 μm). Arrows indicate dopaminergic neurons (green) and p-eIF2α (red) co-stain. (**d**) Summary data showing the ratio of TH+ cells in both the SNc and the VTA that co-labeled for p-eIF2α in eIF2α$^{(S51A/S51A)}$ DAT-Cre vs. WT DAT-Cre control mice (n = 5 mice each, unpaired t test, SNc: $t_{(8)}$= 19.61, P <0,0001; VTA: $t_{(8)}$= 17.19, P <0,0001). (**e,j**) Representative western blots (right panel) and quantification of phosphorylation of eIF2α in VTA (**e**) and SNc (**j**) of eIF2α$^{(S51A/S51A)}$ DAT-Cre and WT DAT-Cre mice. Summary plot showed a robust decrease in the phosphorylation of eIF2α in both VTA (**e**; unpaired t test, $t_{(6)}$ = 4.79, P = 0.003; n= 4 independent lysates from 4 mice per group) and SNc (**j**; unpaired t test, $t_{(6)}$ = 4.54, P = 0.004; n= 4 independent lysates from 4 mice

per group) of eIF2α$^{(S51A/S51A)}$ DAT-Cre mice compared with controls. (**f,k**) Representative western blots (right panel) and quantification of newly synthesized brain proteins in VTA (**f**) and SNc (**k**) of eIF2α$^{(S51A/S51A)}$ DAT-Cre and WT DAT-Cre mice, labelled with puromycin using the SUnSET method (see Methods). Summary plot of puromycilation indicated increased d*e novo* translation in both VTA (**f**; unpaired *t* test, $t_{(6)} = 3.18$, $P = 0.019$; n= 4 independent lysates from 4 mice per group) and SNc (**k**; unpaired *t* test, $t_{(6)} = 5.72$, $P = 0.0012$; n= 4 independent lysates from 4 mice per group) of eIF2α$^{(S51A/S51A)}$ DAT-Cre mice compared with controls. 3-month old eIF2α$^{(S51A/S51A)}$ DAT-Cre mice and their WT DAT-Cre littermates mice were subjected to a set of tests including the bar (**g**), drag (**h**), rotarod (**i**), novel home cage, (**l**) and open field (**m,n**) tests to investigate locomotor activity. (**g**) Summary plot of immobility time (sec) during bar test in eIF2α$^{(S51A/S51A)}$ DAT-Cre *versus* WT DAT-Cre mice (unpaired *t* test, $t_{(19)} = 5.21$, $P < 0.001$). (**h**) Summary plot of average number of steps during drag test (unpaired *t* test, $t_{(19)} = 3.67$, $P < 0.01$). (**i**) Summary plot of latency to fall from the rotating rod measured as average of two days (4 trials/day) test (unpaired *t* test, $t_{(19)} = 1.30$, $P = 0.20$). (**l**) Summary plot of the novelty-induced locomotor activity expressed as a distance moved (cm) in the first 10 minutes interval of a 60 minutes test during novel home cage test (unpaired *t* test, $t_{(19)} = 5.76$, $P < 0.001$). (**m,n**) Summary plot of (**m**) spontaneous locomotor activity expressed as distance moved (cm) and (**n**) vertical activity (number of counts) during the open field test (unpaired *t* test; **m**, $t_{(19)} = 2.78$ $P < 0.001$; **n**, $t_{(19)} = 5.71$ $P = 0.012$). All data are shown as mean ± s.e.m. of $n = 9$ eIF2α$^{(S51A/S51A)}$ DAT-Cre mice and $n = 12$ WT DAT-Cre mice. *$P < 0.05$, **$P < 0.01$ and ***$P < 0.001$ eIF2α$^{(S51A/S51A)}$ DAT-Cre *versus* WT DAT-Cre mice.

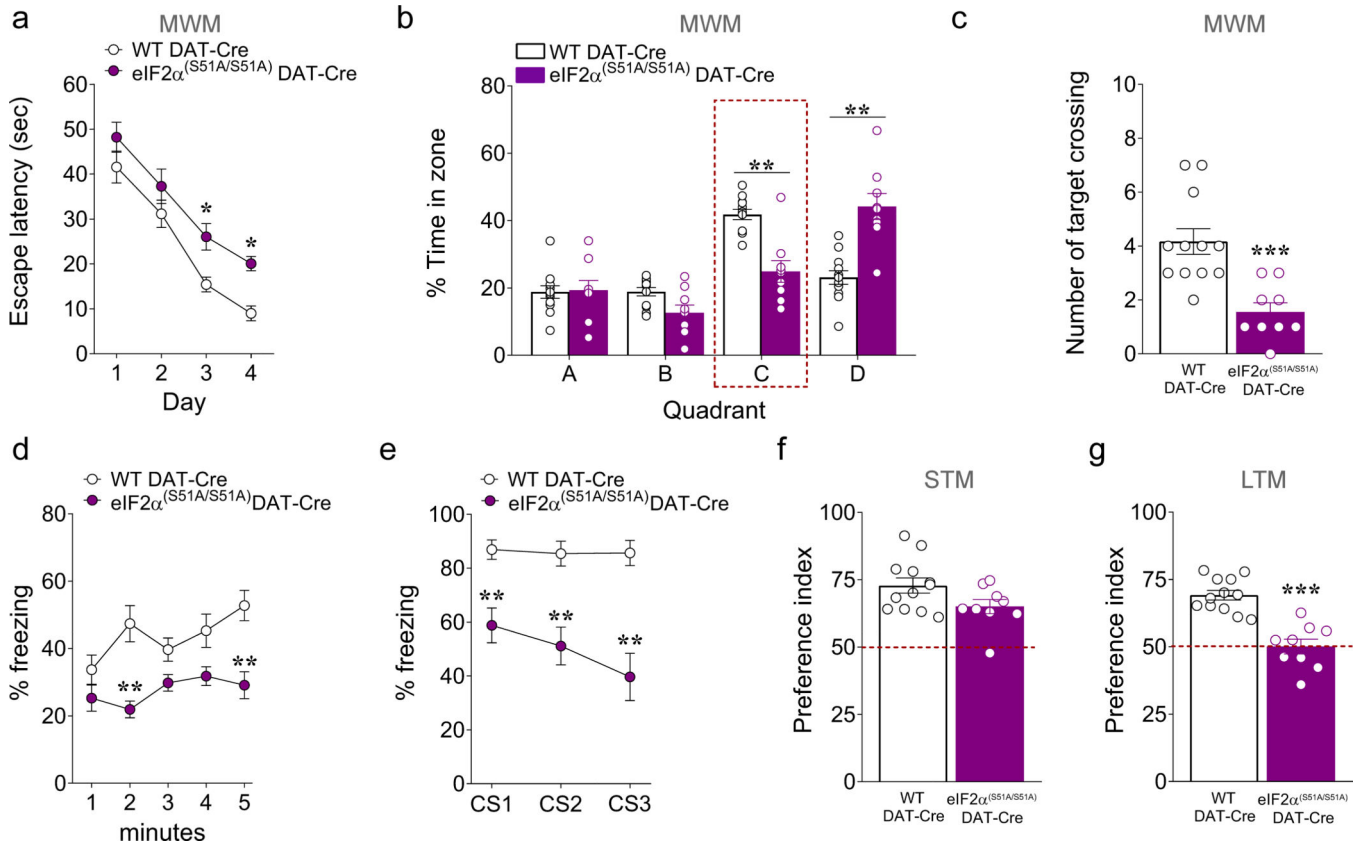

Figure 3. eIF2α$^{(S51A/S51A)}$ DAT-Cre mice display multiple cognitive phenotypes.

(**a-c**) Summary plots of (**a**) average latency to find the hidden platform during a 4-day training protocol, (**b**) percentage spent in each zone and (**c**) average number of times spent crossing the location of the previously hidden platform during probe tests in 3- month old eIF2α$^{(S51A/S51A)}$ DAT-Cre *versus* WT DAT-Cre mice in the MWM test (**a**, two-way RM ANOVA, followed by Bonferroni's multiple comparisons test, time $F_{(3, 57)} = 67.07$, $P < 0.001$, genotype $F_{(1, 19)} = 9.49$, $P < 0.01$; **b**, two-way RM ANOVA, followed by Bonferroni's multiple comparisons test, quadrant x genotype, $F_{(3, 57)} = 17.65$, $P < 0.001$; **c**, unpaired *t* test, $t_{(19)} = 4.193$, $P < 0.001$). (**d,e**) Summary plots of average percentage of freezing during (**d**) exposure to the context 24 hours after training, and (**e**) exposure to 3 CS presentations in a novel context in the associative threat memory test in 3-month old eIF2α$^{(S51A/S51A)}$ DAT-Cre *versus* WT DAT-Cre mice (**d**, two-way RM ANOVA, followed by Bonferroni's multiple comparisons test, genotype, $F_{(1, 19)} = 18.69$, $P < 0.001$; **e**, two-way RM ANOVA, followed by Bonferroni's multiple comparisons test, genotype, $F_{(1, 19)} = 26.76$ $P < 0.001$). (**f,g**) Summary plots of preference indices of mice towards a novel object introduced in the novel object recognition test in 3-month old eIF2α$^{(S51A/S51A)}$ DAT-Cre *versus* WT DAT-Cre mice (unpaired t test; **f**, $t_{(19)} = 1.967$, $P = 0.06$; **g**, $t_{(19)} = 6.017$, $P < 0.001$). All data are shown as mean ± s.e.m. of $n = 9$ eIF2α$^{(S51A/S51A)}$ DAT-Cre mice and $n = 12$ WT DAT-Cre mice. *$P < 0.05$, **$P < 0.01$ and ***$P < 0.001$ eIF2α$^{(S51A/S51A)}$ DAT-Cre *versus* WT DAT-Cre mice.

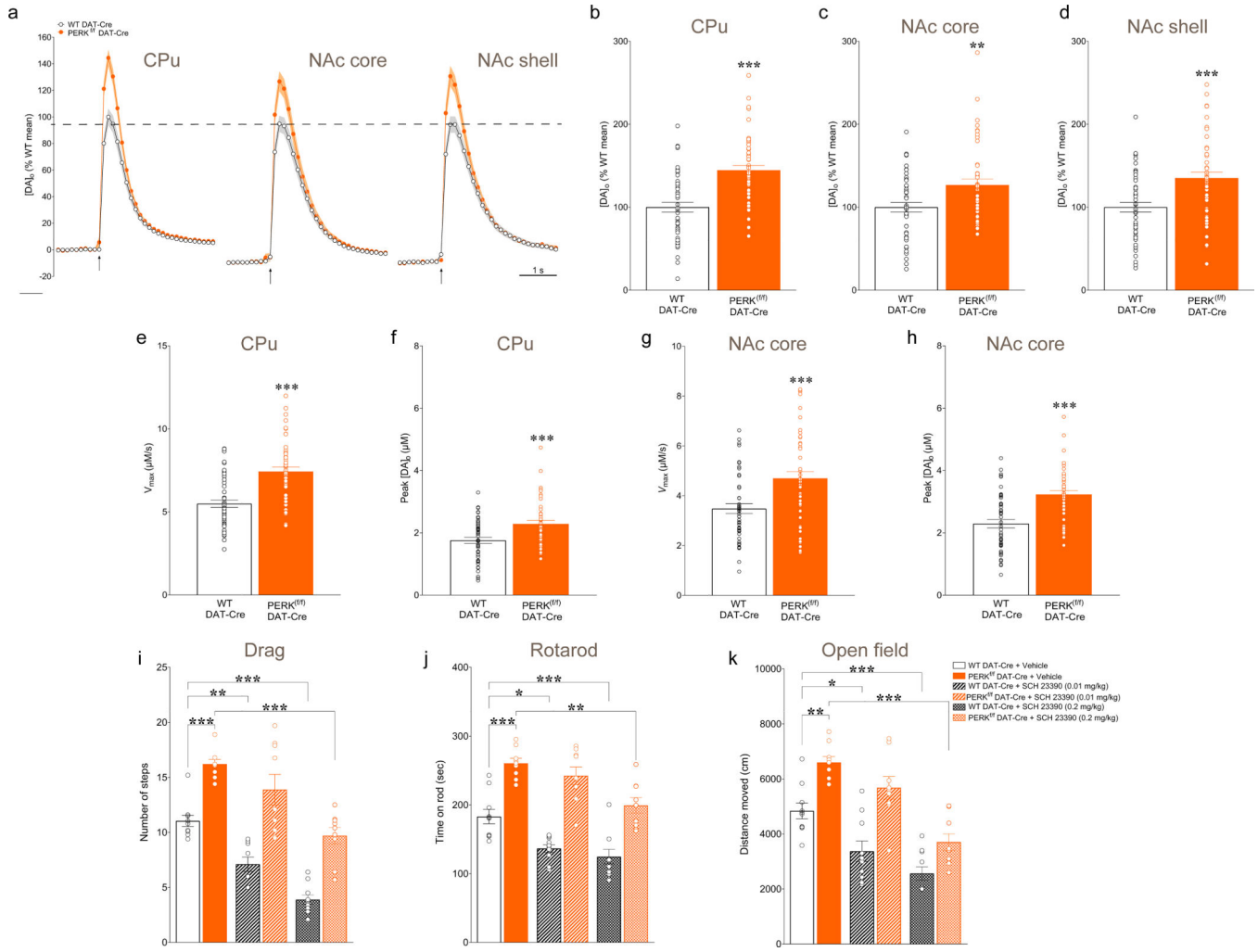

Figure 4. Deletion of PERK in DA neurons alters striatal DA release and DAT activity in mice.

(a) Average single-pulse (1p) evoked $[DA]_o$ transients recorded in CPu, NAc core, and NAc shell in $PERK^{f/f}$ DAT-Cre *versus* control DAT-Cre mice at 3 months of age. (**b-d**) Summary plot of evoked $[DA]_o$ peak expressed as % mean control in CPu (unpaired *t*-test, $t_{(98)} = 5.345$, $P < 0.001$), NAc core (unpaired *t*-test, $t_{(91)} = 2.954$, $P < 0.01$), and NAc shell (unpaired *t*-test, $t_{(97)} = 3.807$, $P < 0.001$) in 3-month old mice. V_{max} values (maximum uptake velocity; **e,g**) and C_{peak} values (peak concentration; **f,h**) for DAT-mediated DA uptake derived from Michaelis-Menten analysis of single pulse evoked $[DA]_o$ records determined using a fixed K_m of 0.9 μM for each brain region and genotype. (**e**) Summary plot of V_{max} values in CPu of WT DAT-Cre *versus* $PERK^{f/f}$ DAT-Cre mice (unpaired *t*-test, $t_{(94)} = 5.589$, $P < 0.001$). (**f**) Summary plot of C_{peak} values in CPu of WT DAT-Cre *versus* $PERK^{f/f}$ DAT-Cre mice (unpaired *t*-test, $t_{(94)} = 5.113$, $P < 0.001$). (**g**) Summary plot of V_{max} values in NAc core of WT DAT *versus* $PERK^{f/f}$ DAT-Cre mice (unpaired *t*-test, $t_{(90)} = 3.616$, $P < 0.001$). (**h**) Summary plot of C_{peak} values in NAc core of WT DAT *versus* $PERK^{f/f}$ DAT-Cre mice (unpaired *t*-test, $t_{(90)} = 3.554$, $P < 0.001$). Data are means ± s.e.m. of *n* mice, where *n* denotes the number of recording sites sampled from 3 to 5 mice per genotype; $^{**}P < 0.01$; $^{***}P < 0.001$ for WT DAT-Cre *vs.* $PERK^{f/f}$ DAT-Cre mice. Values with R^2

< 0.95, indicating goodness-of-fit were excluded from the data reported here. (**i-k**) *In vivo* pharmacological targeting of DA machinery reveals the impact of PERK deletion in DA neurons in mice. Acute i.p. injection of the D1 receptor antagonist (SCH 23390; 0.01 mg/kg) affects locomotor activity phenotype in WT DAT-Cre mice, but does not alter locomotor activity of $PERK^{f/f}$ DAT-Cre mice. Conversely, high-dose SCH 23390 (0.2 mg/kg) impairs locomotor activity in both genotypes. (**i**) Summary plot of average number of steps during drag test (two-way ANOVA, genotype $F_{(1, 51)} = 93.91$, $P<0.0001$, treatment $F_{(2, 51)} = 41.83$, $P<0.0001$). (**j**) Summary plot of latency to fall from the rotating rod measured as average of two days (4 trials/day) test (two-way ANOVA, genotype $F_{(1, 51)} = 112.8$, $P<0.0001$, treatment $F_{(2, 51)} = 18.19$, $P<0.0001$). (**k**) Summary plot of spontaneous locomotor activity expressed as distance moved (cm) during the open field test (two-way ANOVA, genotype; $F_{(1, 51)} = 46.80$, $P<0.0001$, treatment $F_{(2, 51)} = 34.66$, $P<0.0001$). Mice were analyzed using two-way ANOVA followed by the Bonferroni's test for multiple comparisons. $*P < 0.05$, $**P < 0.01$, $***P < 0.001$. All data are shown as mean ± s.e.m. of $n = 10$ (WT DAT-Cre) or 9 ($PERK^{f/f}$ DAT-Cre) mice/treatment.

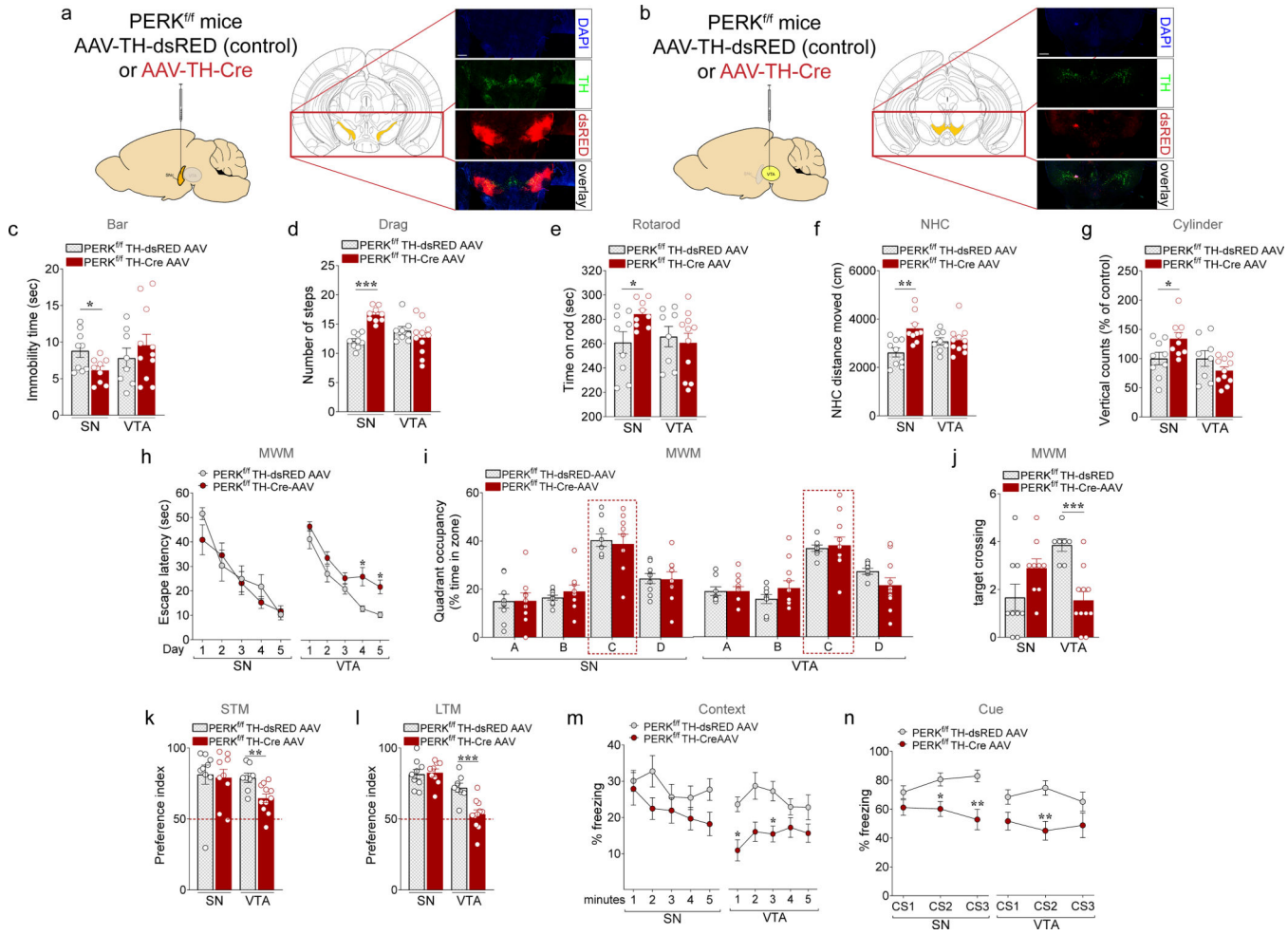

Figure 5. Selective virogenetic deletion of PERK in DA neurons of the SNc or the VTA results in motor or cognitive phenotypes, respectively similar to those displayed by the PERKf/f DAT-Cre mice.

(**a,b**) Schematic for experiments shown in **c-n**. Either AAV2/10 TH-dsRED (control) or AAV2/10 TH-iCre (AAV-TH Cre) was injected bilaterally into (**a**) the SNc or (**b**) the VTA of PERK$^{f/f}$ mice. Representative low magnification immunofluorescence images showing the injection sites (scale bar represents 500 μm). (**c-g**) PERK$^{f/f}$ TH-Cre-AAV and PERK$^{f/f}$ TH-dsRED AAV control mice were subjected to a set of tests including the bar (**c**), drag (**d**), rotarod (**e**), novel home cage (**f**), and open field (**g**) tests to investigate locomotor activity at 3 months of age. (**c**) Summary plot of immobility time (sec) during bar test in PERK$^{f/f}$ TH-Cre-AAV *vs.* PERK$^{f/f}$ TH-dsRED AAV control mice (unpaired *t* test, SN: $t_{(16)} = 2.500$, $P < 0.05$; VTA: n.s). (**d**) Summary plot of average number of steps during drag test (unpaired *t* test, SN: $t_{(16)} = 7.660$, $P < 0.001$; VTA: n.s.). (**e**) Summary plot of latency to fall from the rotating rod measured as average of two days (4 trials/day) test (unpaired *t* test, SN: $t_{(16)} = 2.439$, $P < 0.05$; VTA: n.s.). (**f**) Summary plot of the novelty-induced locomotor activity expressed as a distance moved (cm) in the first 10 minutes interval of a 60 minutes test during novel home cage test (unpaired *t* test, SN: $t_{(16)} = 3.586$, $P < 0.01$; VTA: n.s.). (**g**) Summary plot of vertical activity (number of counts as % of control) during the open field test (unpaired *t* test; SN: $t_{(16)} = 2.300$, $P < 0.05$; VTA: n.s.).. (**h-j**)

Summary plots of (**h**) average latency to find the hidden platform during a 5 training protocol, (**i**) percentage of total time spent in each quadrant, and (**j**) average number of times spent crossing the location of the previously hidden platform during probe tests in 3-month old PERK$^{f/f}$ TH-Cre-AAV *versus* PERK$^{f/f}$ TH-dsRED AAV control mice injected in either SN or VTA in the MWM test (**h**, two-way RM ANOVA, followed by Bonferroni's multiple comparisons test, SN: n.s; VTA: genoype, $F_{(1, 17)} = 15.22$, $P < 0.01$; **i**, two-way RM ANOVA, followed by Bonferroni's multiple comparisons test, quadrant x genotype, n.s., in both SN and VTA; **j**, unpaired *t* test, SN: n.s.; VTA: $t_{(17)} = 4.927$, $P < 0.001$). (**k,l**) Summary plots of preference indices of mice toward a novel object introduced in the novel object recognition test in PERK$^{f/f}$ TH-Cre-AAV *versus* PERK$^{f/f}$ TH-dsRED AAV control mice injected in either SN or VTA (unpaired *t* test; **k**, SN: n.s., VTA: $t_{(17)} = 3.173$, $P < 0.01$; **l**, SN: n.s., VTA: $t_{(17)} = 4.102$, $P < 0.001$). (**m,n**) Summary plots of average percentage of freezing during (**m**) exposure to the context 24 hours after training, and (**n**) exposure to 3 CS presentations in a novel context in the associative threat memory test in PERK$^{f/f}$ TH-Cre-AAV *versus* PERK$^{f/f}$ TH-dsRED AAV control mice injected in either SN or VTA (**m**, two-way RM ANOVA, followed by Bonferroni's multiple comparisons test, genotype, SN: n.s., VTA: genotype, $F_{(1, 17)} = 10.97$, $P < 0.01$; **n**, two-way RM ANOVA, followed by Bonferroni's multiple comparisons test, SN: time x genotype, $F_{(2, 32)} = 5.837$ $P < 0.01$, VTA: time x genotype, $F_{(2, 34)} = 2.79$ $P = 0.075$). All data are shown as mean ± s.e.m. of $n = 9$ PERK$^{f/f}$ TH-Cre-AAV and PERK$^{f/f}$ TH-dsRED AAV mice injected in the SN; $n = 11$ PERK$^{f/f}$ TH-Cre-AAV mice and $n = 8$ PERK$^{f/f}$ TH-dsRED AAV mice injected in the VTA. $^{*}P < 0.05$, $^{**}P < 0.01$ and $^{***}P < 0.001$ PERK$^{f/f}$ TH-Cre-AAV *versus* PERK$^{f/f}$ TH-dsRED AAV mice.